Characterising the response of reinforced concrete cladding panels to vapour cloud explosions

Document Ref: DES07021_090225_V2.0
Issue 2.0: 4 June 2009

Weidlinger Associates Ltd
PO Box 14488
Glenrothes
KY7 6WP
United Kingdom

Tel +44 1383 828270
Fax +44 1383 821682

Website www.wai.com

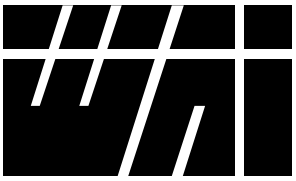

WEIDLINGER ASSOCIATES LTD
CONSULTING ENGINEERS

Authorisation

Prepared by:	CGS
Date:	4 June 2009
Signed:	
Reviewed by:	NKM
Date:	4 June 2009
Signed:	
Authorised by:	PRT
Date:	4 June 2009
Signed:	

Change record

Issue No	Date	Status
1.0	20 March 2009	Initial issue
2.0	4 June 2004	Correction to §6.2 (Preliminary test loadcase reported incorrectly, standoff should be 300m not 100m, associated Figures also updated) Minor correction to para. 11.1.3 (7 loadcases not 8) Minor correction to Figure 56 (curve labels reversed)

Table of contents

1. Introduction

1.1 Background

1.1.1 Ongoing DOSG research into debris throw and collateral damage resulting from explosive storage accidents has focused largely on the effects of a mass detonation of a large quantity of high explosives (HE). In recent studies conducted by Weidlinger Associates the structural response of typical British commercial and residential buildings to blast has been assessed. It has been shown that numerical modelling techniques can accurately predict the response of a range of typical British building types to large scale HE blasts. These studies were in support of work to confirm (or otherwise) current Quantity Distance (QD) standards.

1.1.2 A requirement has now been identified to investigate the response of British commercial buildings to blasts resulting from hydrocarbon vapour cloud explosions. The nature of the loading from this type of blast is significantly different from that resulting from an HE blast and the structural response to this loading is also likely to be different.

1.1.3 This study examines the response of typical reinforced concrete façade cladding panels (RC panels) subjected to blast loads of a form consistent with vapour cloud explosions.

2. Scope

2.1.1 This task concerns the analysis of a typical reinforced concrete façade cladding panel subjected to blast loads of a form consistent with vapour cloud explosions.

2.1.2 The primary purpose of this task was to generate Pressure-Impulse (PI) iso-damage curves for the structural component concerned by using the same numerical modelling techniques as were used in the previous studies for DOSG involving structural response to HE blast.

2.1.3 Pressure-impulse iso-damage curves were to be generated using a range of loading forms in order to asses the variability of the structural response to different types of blast.

2.1.4 For the purposes of this investigation a generic structural reinforced concrete cladding panel was to be analysed. This type of cladding is common in British commercial building construction but has not been considered in previous studies where steel frames and structural masonry where of primary interest.

2.1.5 A large quantity of data is available regarding the performance of offshore oil and gas installations when subjected to confined or partially confined vapour cloud explosions. However, due to the complexity of modelling and physical testing of vapour cloud explosions, there is very little data available regarding the performance of land based structures, commercial or domestic residential buildings for example, subjected to unconfined or partially confined vapour cloud explosions. In order to provide a known point of reference when conducting this assessment a particular structural arrangement was to be analysed based upon a real structure which was subjected to an accidental large

vapour cloud explosion.

3. The structural component to be assessed: precast RC cladding panel

3.1.1 Precast reinforced concrete cladding panels are widely used in the British construction industry. These panels generally form the exterior of a building and are therefore part of the architecture of the building and not just a structural component. The result is that the form and appearance of these panels can vary significantly. To reduce weight these panels can have void spaces or can be constructed with a beam grillage supporting a thinner slab. Sometimes the exterior surface concrete will be coloured, textured or patterned for aesthetic reasons. Commonly these panels are faced with brickwork. However, the underlying structural behaviour is reasonably consistent amongst the range of cladding styles. Generally, the cladding panel is simply a reinforced concrete slab attached to the primary structure on two or more sides.

3.1.2 In order to provide a known point of reference when conducting this assessment a particular structural arrangement was to be analysed based upon a real structure which was subjected to an accidental large vapour cloud explosion. The structure chosen for this analysis was the Northgate building (Northgate House) in Hemel Hempstead. This building was subjected to a large vapour cloud explosion resulting from an accident at the Buncefield oil storage and transfer depot, Hemel Hempstead, on 11 December 2005. A full description of the damage to this building, and the accident which caused the damage, is beyond the scope of this study. This assessment only considers the reinforced concrete panels which were used to clad the outside of the Northgate building.

3.1.3 The cladding panels used on the Northgate building were typical of those used throughout Britain in commercial/industrial buildings. The primary panel structure consisted of a reinforced concrete slab approximately 7m long by 2.2m high by 0.36m thick and spanned horizontally between the columns of the supporting structure. Along the top and bottom of the slab there were thicker beam sections which were more heavily reinforced than the slab itself. Spanning vertically between the two beam sections there were concrete "ribs" which defined a number of void spaces which were filled with a lightweight foam. The panels were faced with brickwork which was supported on a steel angle section which was itself anchored onto the bottom beam section of the panel. Figure 1, Figure 2 and Figure 3 show views of these cladding panels after the accident.

3.1.4 The most interesting feature of the response of these panels during the blast was that two different batches of panels exhibited significantly different responses. There was one set of panels which showed only minor damage while another set of panels showed heavy damage. The heavily damaged panels showed what would be considered a failure in the form of a severe crack running vertically at midspan.

3.1.5 Figure 4 shows a side-by-side view of what will be referred to in this report as the "strong" and "weak" panels. The panels of interest are those on the top storey of the Northgate building. The damaged panels, an example of which is shown on the right of Figure 4, retained a permanent midspan deflection of approximately 200mm. The 200mm estimate was derived from the image shown in Figure 5 as well as from verbal accounts. The vast majority of the panels remained intact and attached to the supporting structure but the exterior brickwork was heavily damaged.

3.1.6 Subsequent investigations revealed that the two batches of cladding panels had been installed at different times. Structurally the panels appeared to be identical but closer inspection indicated that the panels which received only minor damage had slightly more reinforcing steel than those panels which received heavy damage (the "strong" and "weak" panels respectively).

3.1.7 The cladding panels were located on three storeys of the building but only panels on the top floor failed. The panels on the lower floors were supported by floor slabs as well as by the main structural columns. This additional restrained appears to have prevented the panels from failing.

3.1.8 This damage pattern was observed over a large number of panels covering most of the presented face of the building. This means that the observed damage pattern was not a local response and not a result of minor variations in workmanship between panels.

3.1.9 It was also concluded from the observed damage to the whole building and the surrounding area that all of the panels in question would have received a similar level of pressure loading from the blast. However, the Buncefield Accident Investigation has yet to be able to determine conclusively what the form or magnitude of the blast loading was in this location.

3.1.10 This situation provides a unique opportunity to investigate the response of reinforced concrete cladding panels to vapour cloud explosions. The fact that there were two almost identical panel designs subjected to the same large vapour cloud explosion yet exhibiting significantly different responses provides a means of bracketing the magnitude and form of the blast loading that would have been required to cause this very specific damage pattern. It also provides a known reference point to which a range of other load scenarios could be referenced to; blast loads from high explosives rather than vapour clouds for example.

4. Important assumptions

4.1 Input data

4.1.1 As with any investigation of the type conducted here information regarding the structure analysed, and the event which caused the damage, was incomplete. As a result it was necessary to make assumptions and estimates to fill gaps in the available data. The main assumptions regarding the structural definition of the cladding panels are listed and described below.

4.2 List of assumptions

4.2.1 It was assumed that the panels were normally reinforced but not prestressed or post-tensioned. Photographs of the panel reinforcement shows what appear to be normal steel reinforcement bars rather than prestressing tendons/conduits. If the panels were prestressed, which seems unlikely, the results of this analysis could be significantly different

4.2.2 No material specification was available for the concrete. Structural cladding panels of the

form seen here would typically be cast in C30 or C40 concrete or a customised mix for aesthetic purposes but with an unconfined compressive strength in the 30MPa to 40MPa range. It has been assumed that a conventional C40 mix has been used. The compressive strength of the concrete is likely to have little influence on the results of this analysis since most of the observed damage to the panels was through tensile cracking of the concrete and yielding of the reinforcement. The tensile properties of the concrete have been assumed to be for a typical C40 mix.

4.2.3 It was assumed that the same or similar concrete mix has been used for all of the panels.

4.2.4 The specification of the reinforcement steel is not known; primarily whether it was mild steel or high yield steel. The difference between these could have a significant influence on the results. Either option seems equally possible but it would be difficult and time consuming to consider all variations of material specification for each set of reinforcement bars. For the purposes of the hand calculations both a mild steel and a high yield steel were considered with yield stresses of 250MPa and 460MPa respectively. For the purposes of the finite element analysis a compromise material specification was used for all reinforcement steel where it was assumed that that the steel yields at a tensile stress of 250MPa (similar to a mild steel) but reaches an ultimate stress of 460MPa (similar to a high yield steel) at around 10% elongation. Given this approximation it was considered unnecessary to include rate effects in the steel material model.

4.2.5 No material properties were available for the steel angle section. It was assumed that this angle section was a 200x100x12 RSA section in steel with a yield of 275MPa.

4.2.6 No material properties were available for the foam used in the void spaces within the RC panel. It was assumed that this foam was structurally insignificant. It was not included in the hand calculations but was included in the finite element model as a linear elastic material with low strength and stiffness compared to the surrounding concrete.

4.2.7 No material properties were available for the masonry which formed the exterior surface of the cladding panel. Typical properties were used based upon previous work for DOSG.

4.2.8 It was assumed that there was no significant tensile structural connection between the masonry and the concrete and that the masonry was supported only by the steel angle section. It is known that there were masonry wall ties connecting the masonry to the vertical concrete ribs on the panel. However, from experience of this type of analysis it can be said that the wall ties would break loose of their fixings in the mortar during the positive phase of the blast and would have only minimal influence on the overall response of the structure.

4.2.9 The details of the connection between the panels and the supporting structure were unknown. It was assumed that the panels were simply supported. This assumption is consistent with the observed deformed shape of the damaged panels.

4.2.10 It has been assumed that the concrete in the panels was initially un-cracked before the blast.

4.2.11 It has been assumed that the blast loading was a uniform pressure applied to the external face of the brickwork. These loads would be transmitted through to the concrete via a 10mm thick layer of mortar and through compression-only contacts between the masonry and the concrete, and to a lesser extent through the infill foam. It has been assumed that any pressure applied to the inside face of the panel, *i.e.* from pressure rise inside the building, was low relative to the external pressure.

4.2.12 It has been assumed that the failed panels were unrestrained after failure except at the supports, *i.e.* the back face of the failed panels at midspan did not come into contact with the supporting structure behind.

5. Initial strength assessment: hand calculation

1.1 Hand calculation

5.1.1 The primary means of calculating the structural response in this study was through detailed finite element analysis and simplified single-degree-of-freedom (SDOF) modelling. However, some simple hand calculations were used to provide an additional estimate of the strength of the cladding panels as well as to provide a verification of the model predictions. These hand calculations are presented at Annex A along with a description of the geometry and reinforcement details used in this assessment. The primary results of these calculations are described below.

5.1.2 The hand calculations were conducted in order to determine the strength of the panels when resisting a statically applied uniform pressure on the external surface of the panels.

5.1.3 It has been assumed that the panels were uncracked and undamaged before the blast. Therefore the applied pressure at which the concrete on the back face of the panel cracks is of interest. The hand calculations indicate that the concrete on the back face of the panel would crack at an applied uniform pressure of approximately 12.9kPa. This value is the same for both the weak and the strong panels.

5.1.4 Once the concrete has cracked all of the tension in the back of the panel would be carried by the reinforcing steel. It has been calculated that if mild steel reinforcement was used the steel on the back face of the panel would yield at an applied uniform pressure of 5.0kPa for the weak panel and 9.0kPa for the strong panel. Clearly these values are less than the pressure at which the concrete would crack. This would suggest that failure of the panel would be sudden but ductile under a constant uniformly applied pressure loading. Typically the tensile strength of the concrete would be neglected in structural design but it has been included in this analysis.

5.1.5 Similarly, the steel in the strong panel would yield at an applied pressure of approximately 8.4kPa or 15.5kPa for mild steel and high yield steel respectively.

5.1.6 These estimated pressures to initiate failure of the panels are quite low (*i.e.* the panels are not very strong when resisting blast compared to typical structural columns/beams for example). To illustrate this it is possible to devise a TNT scenario which would produce a peak pressure high enough to *initiate* failure of the panels. For example, a 28kg TNT high explosive charge would produce a peak pressure of 15.5kPa at a standoff of 50m. This

would not be considered a particularly severe loading in most blast engineering problems. It should be noted that cracking of the concrete on the rear of the panel does not indicate failure but indicates onset of damage.

6. Strength assessment: finite element analysis

6.1 Software - NL FLEX

6.1.1 The structural analysis software used in this task was the Weidlinger Associates code FLEX. FLEX is a non-linear explicit finite element code developed and used by Weidlinger Associates to specifically address high severity loadings on buildings, facilities and structures.

6.1.2 FLEX has a large library of elements and constitutive models that are tailored to the solution of large, transient non-linear problems through to failure. Material models may be either linear elastic or non-linear and both two and three invariant plasticity models have been developed to represent the non-linear behaviour of metals, soil, rock and reinforced concrete.

6.1.3 FLEX has been benchmarked against other modelling frameworks and validated through pre-test prediction comparisons of blast and fragmentation problems with small scale and full-scale tests. Additional information on FLEX, its constitutive models and various validation studies are detailed in References 6 to 28.

6.2 Preliminary analysis to confirm failure mode and validity of assumptions

6.2.1 The primary means of calculating the strength of the cladding panels in this study was by non-linear finite element analysis.

6.2.2 It has been explained previously that a degree of "engineering judgement" was required in order to fill the gaps in the input data regarding the structural definition of the cladding panels. The first finite element analysis step of this assessment was to conduct a high fidelity, fully dynamic non-linear analysis of the response of a cladding panel to a large but distant TNT explosion. The purpose of this analysis was to confirm that the data available regarding the structural definition of the panels combined with the assumptions that had to be made could be used to build a finite element model which would produce a qualitatively realistic structural response to a realistic dynamic blast loading.

6.2.3 Figure 6, Figure 7 and Figure 8 show the geometry of the finite element model used for this analysis. The model only includes a single cladding panel with reinforcement arranged to model the "weak" panel.

6.2.4 Figure 6 shows the geometry of the concrete only part of the model. Clearly visible are the horizontally spanning beam-sections at the top and bottom of the slab. Also visible are the seven void spaces which are filled with a type of foam as well as the vertical ribs separating them and supporting the exterior brickwork.

6.2.5 Figure 7 shows a similar view but with the infill foam and the steel angle sections also shown. It was not known whether there was an angle section at the top of each panel as

well as at the bottom, so for symmetry it has been assumed that there was a steel angle section at the top and bottom.

6.2.6 Figure 8 shows the full model including the facing brick. It should be noted that the material properties of bricks and mortar can vary significantly and still be within a standard specification. However, the strength of the brickwork is unlikely to have a significant influence of the results of this assessment since most of the strength of the panel comes from the reinforced concrete sections.

6.2.7 Figure 9 shows a view of the finite element discretisation used in this model. The concrete, bricks and mortar were modelled with 8-noded iso-parametric hexahedral elements. A total of 424,306 hexahedral elements were used with a nominal size of approximately 15mm.

6.2.8 There were no details available regarding the material properties of the bricks and mortar used in the construction of the cladding panels. Typical properties for the bricks and mortar were used according to previous studies conducted for DOSG where the response of brickwork was of primary concern, Reference 5. The FLEX "sft1" material model was used for the concrete, brick and mortar materials in the cladding panel structural models. This constitutive model is a three-invariant viscoplastic softening model designed to replicate the concrete material characteristics reported in CEB-FIP model code 1990, Reference 1, but which can be easily modified to model other quasi-brittle materials (such as brick and mortar).

6.2.9 The infill foam was treated is an elastic-ideally-plastic material using a von Mises isotropic hardening plasticity model with a stiffness 100 times less than concrete and a strength of 0.1MPa.

6.2.10 Figure 10 shows the reinforcing mesh used in this model. 2-node iso-parametric beam elements were used to model the reinforcement bars.

6.2.11 4-node isoparametric quadrilateral layered shell elements were used to model the steel angle sections with 4 through-thickness layers.

6.2.12 A simple von Mises isotropic hardening plasticity model was used for the steel components in this model. The steel angle section was assumed to be elastic-ideally-plastic with a yield stress of 275MPa. A softening curve was also defined beginning at an elongation of 18% but this region of the response would not be used in this analysis.

6.2.13 The model used for the reinforcement steel was slightly different. As stated previously, it was not known whether mild steel or high yield steel was used in the cladding panels. It was not practical to do every analysis twice so a hybrid model has been used as a best-estimate model. It has been assumed that the steel yields at a stress of 250MPa and reaches an ultimate stress of 460MPa at a strain of 10%. Again a softening curve was also included, beginning at 18% strain.

6.2.14 The precise details of the connection between the cladding panels and the supporting structure were not known. However, it could be seen from the response, the failure mode, and from the image in Figure 3 that the ends of the panels were essentially simply

supported (on the upper storey only; additional restraints existed at lower floors). In order to replicate this support condition a pair of end-bearing-pads were build into the model. These are shown Figure 11. Figure 11 is a view if the rear of the panel. The end-bearing-pads are shown in blue. The end-bearing-pads were defined as a linear elastic material with properties similar to the concrete of the panel. The rear face of the end-bearing-pads were treated as rigid and constrained to give simply-supported conditions for the panel.

6.2.15 The purpose of this preliminary analysis was to confirm that the known input data combined with the assumed input data would produce a realistic response to a realistic loading. Unfortunately, not knowing what the actual loading was makes it quite difficult to decide what would be a realistic blast loading for this test case. The aim of the analysis was to cause the panel to fail without completely destroying it (*i.e.* within a similar damage category as was observed. For this analysis a loading equivalent to a 100Tonne TNT charge at a standoff of 300m was chosen. It was known, from experience, that this would fail the panel and probably be significantly more severe than the actual loading, but not so severe as to completely destroy the panel.

6.2.16 Figure 12 shows a snapshot of the deformed shape of the panel during the test run. Clearly the mode of failure is a vertical cracking of the concrete at midspan. This is obviously very similar to that observed on-site as shown in Figure 5 except that the masonry has not been removed. Figure 13 shows contours of damage to the structure (with red being fully damaged and blue being completely undamaged). The parameter plotted in Figure 13 is "volumetric damage" and represents the combined effects of volumetric strain and overall material damage. Figure 14 gives probably the clearest view of the failure mode. In Figure 14 only the concrete part of the cladding panel is shown with the vertical cracking near midspan clearly visible. Figure 15 shows contours of panel displacement clearly showing the mid-span deflection.

6.2.17 It is important to note at this point that the failure mode is not a shear failure at the supports but is a flexural failure. In general it can be said that a short duration high intensity loading (relative to the natural frequency and strength of the structure) tends to produce a shear failure. A long duration low intensity loading tends to produce a flexural failure. The region between these two extremes tends to produce a combined shear/flexural failure. The fact that the failure mode is purely flexural would suggest that the duration of the applied loading, for the test run as well as during the real blast, was long relative to the natural frequency of the structure. A simple hand calculation would suggest that the natural frequency of the cladding panel would be around 15Hz and that the period would be around 70msec for the uncracked section. The flexural failure mode would suggest that the applied loading had a period of significantly greater than 70msec. The positive phase duration of the 100Te TNT test blast at 300m was around 193msec.

6.2.18 The conclusion of this preliminary analysis is that the behaviour of the finite element model, based upon the available input data as well as upon assumed data where necessary, produces a qualitatively realistic response to a realistic dynamic blast load. This gives a degree of confidence that the input data was qualitatively correct. Further validation of the finite element model will be described below.

6.3 Pseudo-static analysis to calculate pressure-deflection curves

6.3.1 The aim of this assessment was to evaluate the response of the cladding panels to a wide range of blast loads. However, to conduct the type of high fidelity dynamic finite element analysis described above is a computationally intensive exercise. This makes it unpractical within the available time to conduct a useful number of analyses at such a high fidelity.

6.3.2 For this assessment it was necessary to develop fast-running, but still accurate, models of the panels. These models were based upon a single-degree-of-freedom methodology whereby the dynamic behaviour of the structure is represented by a simple spring-mass-damper system. A primary requirement of this type of model is that the load-deflection response of the structure in question is known.

6.3.3 The SDOF models for this assessment are based upon the pseudo-static load-deflection response of the panels. This assumption would not be valid if the applied load was in the high-intensity-short-duration regime. The flexural failure mode observed on-site indicates that the applied loading was in the low-intensity-long-duration regime so the pseudo-static assumption is valid in this case.

6.3.4 The hi-fidelity finite element model was too computationally expensive to conduct a pseudo-static analysis so a coarser model was developed. This model takes advantage of the symmetry of the structure, the symmetry of the failure mode, and the purely flexural nature of the failure mode. The resulting geometry model and finite element mesh is shown in Figure 16 and Figure 17. This model is similar in every way to the high fidelity model except for the mesh resolution and the symmetry conditions. However this model only uses 17,909 hexahedral elements compared to the 424,306 elements used in the high resolution model. Since the actual failure mode is known to be a flexural failure at midspan the resolution of the model can be reduced without adversely affecting the result. The initial analysis had to be at a higher resolution in order to avoid having an undue influence on the failure modes that could be found in the test case.

6.3.5 Instead of applying a blast load to this model a gradually ramped load was applied in order to determine a load-deflection response. In this assessment the post-peak response of the structure was of significant interest. Therefore it is necessary to use a displacement-controlled applied loading instead of load-controlled loading which would have been easier to apply. Applying a displacement controlled uniform pressure loading to a non-uniformly displacing structure is not a trivial exercise. The method used here was to apply (numerically) a fluid filled bladder to the external face of the structure being loaded. This bladder is compressed by displacing its boundary at a constant rate. As the bladder compresses the pressure inside increases as does the pressure applied to the structure. When the structure fails it displaces and relieves the pressure in the bladder and the pressure applied to the structure reduces. In this way it is possible to determine the post-peak response of a non-uniformly deforming structure under a uniformly distributed applied pressure.

6.3.6 Two finite element models were developed for this part of the study with different levels of reinforcement defined in order to model the weak and the strong cladding panels. A ramped pseudo-static uniformly distributed pressure was applied to each model using the displacement-controlled method described above. The load-deflection responses of the panels were recorded and the results are shown in Figure 18.

6.3.7 Figure 18 shows the applied pressure versus the deflection at midspan for the weak and strong panels. The primary features of these curves are as follows:

- The initial response is almost linear elastic, up to a deflection of approximately 6.5mm.
- At a deflection of approximately 6.5mm the concrete on the back face of the panel cracks.
- The tensile load on the back face of the panel is immediately taken up by the reinforcing steel which immediately yields.
- As the steel yields it hardens up to its ultimate stress which occurs at a panel deflection of approximately 25mm at which point the load-deflection curve plateaus.
- The initial responses of the weak and strong panels are similar.
- The plateau for the strong panel is approximately 25% higher than for the weak panel.

6.3.8 The features described above are all explainable and are consistent with what would be expected so qualitatively the responses predicted by the finite element analysis are correct. However, for further verification Figure 19 shows an overlay of the maximum yield levels predicted by hand calculation compared to those predicted by the finite element analysis. Generally, the hand calculations and the finite element calculations produced very similar results giving a degree of confidence that the results are valid within the bounds of the assumptions that have been made.

6.3.9 The sharp step in the load deflection curve at the point where the concrete cracks is probably not significant for this assessment but it has been included in the SDOF models in case there were any unexpected consequences of such a feature. Figure 20 and Figure 21 show overlays of the finite element predicted pressure-deflection curves with the idealised pressure-deflection curves which would be used in the SDOF models for the strong and weak panels respectively.

6.3.10 Figure 22 shows the final form of the pressure-deflection curves to be used in the SDOF models for the strong and weak panels. Clearly the primary difference between these to curves is that once the concrete cracks the stronger panel is approximately 25% stronger than the weak panel, primarily due to the quantity of reinforcement.

7. Single-degree-of-freedom (SDOF) model development

7.1 Background

7.1.1 SDOF models are commonly used in protective design/analysis problems where the requirement is for fast running but accurate nonlinear dynamic response calculations. Typically they would be used to assess the response of building components, columns, beams, floors, glazing systems *etc.* to a wide range of threats. For example, a range of

threats would need to be considered and at a rage of standoffs. Then a range of structural components and retrofit options would need to be assessed against each of these scenarios. Very quickly the parameter space that needs to be considered becomes very large. The purpose of a SDOF model is to allow this type of analysis to be conducted in a matter of hours rather than in the weeks or months that would be required to conduct a full range of high fidelity finite element analysis.

7.1.2 The application here is similar. There are only two structural components to be assessed but the applied loading is completely unknown. If the vapour cloud ignited and then deflagrated the blast loading would be a relatively smooth curve of relatively long duration. If a transition to detonation took place then the blast loading would include a very sharp shock wave with a slow gradual decay. A range of intermediate regimes could also be possible. These options consider the form or shape of the blast loading curve. The magnitude of the blast loading also needs to be considered. The result is that a very large number of analyses would need to be conducted in order to fully investigate the wide range of possible applied loads. The SDOF modelling methodology allows this to be done within practical timescales.

7.2 SDOF models for the RC cladding panels

7.2.1 SDOF models have been developed for each of the two cladding panel designs being considered. The primary purpose of the finite element analysis above was to provide load-deflection curves for the cladding panels for use in the SDOF models being described here.

7.2.2 The basic SDOF model used here assumes that the structure is linear elastic up to the point where the concrete cracks. Once the concrete cracks the steel yields immediately. Once the steel begins to yield it is assumed that any additional deformation is permanent plastic deformation. The unloading stiffness is assumed to be the same as the initial stiffness which is not entirely accurate but is accurate enough for this analysis. The resistance-function for the SDOF spring is based upon the load-deflection curves obtained from the finite element analyses.

7.2.3 The SDOF model used here also includes a viscous damper component. Damping is always a difficult feature to estimate accurately. Typically values between 2% and 10% of critical at the natural frequency of the structure would be used depending upon the type of structure. Most of the damping in the structure being considered here is from internal material behaviour rather than from external factors as would be the case for a larger structure. The constitutive model used for the concrete, mortar and bricks in the finite element analysis included viscous effects as well as cracking and failure behaviour. As a result the finite element model also replicates the damped behaviour of the structure quite well without having to add artificial viscosity. The dynamic response of the finite element model was used to estimate an appropriate damping factor for the SDOF models. A damping factor of 4% of critical damping at the natural frequency of the uncracked panel was found to give a realistic response.

7.2.4 Choosing a mass to be used in the SDOF models is also not a straightforward exercise. The whole panel, including the masonry, has a mass of approximately 12,000kg. However, not all of this mass is "effective mass". The pressure load applied to the panel is acting against the inertia of the panel to produce an acceleration and a displacement.

But the panel is restrained at its edges so the mass at the edges and its inertia does not have a significant influence on the motion of the panel. The result is that the mass used in the SDOF model is typically less than the mass of the whole panel. The mass factor which relates the mass used in the SDOF model to the total mass of the structure varies with the type of structure, its boundary conditions and the expected failure mode. For a simply supported beam or slab which is expected to fail in flexure a mass factor of 0.33 is usually used. This factor can be derived analytically and is related to the deformed shape of the failed structure.

7.2.5 The method of using an SDOF model to represent a structure is comprehensively described in References 2,3, and 4.

8. Applied loads

8.1 Background

8.1.1 Perhaps the biggest unknown variable in this study is the form and magnitude of the blast pressure loads which were actually applied to the Northgate building.

8.1.2 Investigators have argued that if the vapour cloud ignited and then deflagrated the blast loading would be a relatively smooth curve of relatively long duration. If a transition to detonation took place then the blast loading would include a very sharp shock wave with a slow gradual decay. A range of intermediate regimes could also be possible particularly if there were multiple ignition points within the cloud. The purpose of this study was to investigate the response of the cladding panels to as many of these variations in load as possible.

8.1.3 Four basic forms of loading have been selected for this assessment. Each of these loads has been defined by a unit load curve which produces a peak pressure and a total impulse of one unit. Each of these unit load curves is then scaled to give a wide range of peak pressure and impulse combinations while maintaining the basic shape of the load curve.

8.1.4 A total of 160,000 loadcases were considered in the full set of SDOF analyses.

8.1.5 It can be predicted in advance that most of the damage to the structure will occur during the positive phase of the blast loading. The masonry facing on the cladding panels and its weak connection to the concrete effectively isolate the concrete slab response from the negative phase of the blast loading. If there was a significant negative phase to the blast loading it would tend to strip the masonry from the cladding panels without transferring significant load into the concrete. For this reason only positive phase loads have been considered in the SDOF analyses.

8.2 Vapour or gas cloud explosion (Assumed Blast Load A)

8.2.1 The most obvious choice of an applied load would be a form consistent with a "typical" vapour or gas cloud explosion. Typically, a confined or partially confined vapour cloud explosion would result in load curve characterised by a finite rise time, a smooth peak and a long decay which depends upon the degree of venting. Although the Buncefield vapour cloud was unconfined, the general form the load curve could be similar to that of a

partially confined blast.

8.2.2 The first form of loading considered in this study is one which is of a form similar to a partially confined vapour cloud explosion. The curve used consists of a sinusoidal finite rise in pressure followed by an exponential decay. It has been assumed that the rise time is 30% of the total blast duration with the decay being 70% of the duration. The unit-load-curve used is shown in Figure 23.

8.3 Idealised high explosive blast (Assumed Blast Load B)

8.3.1 Another possibility is that there was a rapid transition to detonation resulting in a load curve which looks more like the blast loading resulting from a high explosive.

8.3.2 The second form of blast loading considered in this analysis is a triangular load with zero rise time and a linear decay as shown in Figure 24.

8.4 Assumed Blast Load C

8.4.1 It is much more difficult to define the intermediate forms of loading because there are infinite possible variations.

8.4.2 However the third and fourth type of blast loads considered here are based upon an assumed feasible behaviour of the vapour cloud. If the vapour deflagrated resulting in a long duration low intensity load then transitioned to detonation locally when the flame front reached the Northgate building (the vapour cloud formed around the base of the building) then the load curve could end with a sharp pressure spike. This assumed load curve is shown in Figure 25.

8.5 Assumed Blast Load D

8.5.1 Alternatively there could have been a partial detonation within the cloud resulting in an initial sharp pressure spike followed by a long duration low intensity deflagration. The result would be load curve which looked something like the curve in Figure 26.

8.6 General comments about the choice of blast loads

8.6.1 Clearly there have been some significant assumptions made in order to define the range of applied loadings. However, the forms of loading chosen for analysis cover a wide range of possibilities and include most of the potential phenomena which may have occurred.

8.6.2 These load curves were chosen to allow general conclusions to be made about the response of the structure to different forms of loading rather than to specific loads.

8.6.3 If the results of CFD analyses conducted by other investigators were available then it would be a relatively straightforward exercise to assess the structural response using the SDOF models developed here. A total of 160,000 loadcases were analysed here so a small number of specific load curves resulting from detailed CFD analyses of the vapour cloud behaviour could be assessed quite easily.

9. Generating pressure-impulse diagrams and iso-damage curves

9.1 Methodology

9.1.1 Each of the four unit load curves was scaled repeatedly to give a range of peak-pressure/total-impulse combinations. The range of pressures considered was from 0kPa to 50kPa. The range of impulse considered was 0kPa.s to 50kPa.s. This parameter space was discretised on a grid of 200 pressures by 200 impulses to give a total of 40,000 combinations. The ranges to be analysed were selected based upon the results of initial analysis runs as well as an assumption that the duration of the blast was certainly not more than a few seconds.

9.1.2 Each of these scaled load curves was used as an input loading to each of the panel SDOF models and the final predicted permanent deflection of the structure was recorded. For each of the two panels (weak and strong), and for each of the four load types, a contour plot of permanent deflection versus pressure and impulse was generated.

9.1.3 Each of these contour plots represents a concise and comprehensive response function for all scales of loads of each particular assumed form. To turn these into iso-damage curves it is necessary to extract discrete contours from each plot at specific deformation levels.

9.1.4 Once these iso-damage curves have been generated it is possible to compare directly the response the observed and predicted responses of the weak and strong panels to each load type.

9.1.5 The primary feature of interest in these plots would be if it could be shown that the iso-damage curve representing a 200mm permanent deflection of the weak panel actually crossed the iso-damage curve for minimal damage of the strong panel. The point where the two curves crossed would represent an actual load curve which would produce the same structural response as was observed on-site after the explosion.

9.1.6 In this way it would be possible to determine the form and magnitude of the load which actually resulted from the Buncefield explosion. If this information could be determined it would also aid in explaining the mechanisms involved in the vapour cloud explosion itself.

9.2 Results

9.2.1 The results of the SDOF analyses for each load type are presented in three ways. The continuous pressure-impulse diagrams, the discrete iso-damage curves, and the iso-damage curves specifically for a 200mm permanent deflection of the weak panel and for minimal damage of the strong panel are all presented. Table 1 lists the figures where the results of the SDOF analyses are presented.

	Continuous pressure-impulse diagram		*Discrete iso-damage curves*		*Iso-damage curves for 200mm weak panel deflection & strong panel damage onset*
	Strong panel	***Weak Panel***	***Strong panel***	***Weak Panel***	
Vapour cloud explosion (A)	Figure 27	Figure 28	Figure 29	Figure 30	Figure 31
HE explosion (B)	Figure 32	Figure 33	Figure 34	Figure 35	Figure 36
Assumed load C	Figure 37	Figure 38	Figure 39	Figure 40	Figure 41
Assumed load D	Figure 42	Figure 43	Figure 44	Figure 45	Figure 46

Table 1; List of figures showing results of SDOF analyses.

10. Discussion and interpretation of results

10.1 Comparison of results for onset of damage to strong panel and failure of weak panel

10.1.1 Onset of significant damage to the strong panels has been assumed to occur at a permanent deflection of 30mm. This would be consistent with cracking of the concrete without significant permanent deformation. A deflection greater than 30mm would have been obvious on-site. The position of the iso-damage curves are quite widely spaced in the 0mm to 30mm deflection region along the pressure axis. Above a deflection of 30mm the iso-damage curves are quite closely spaced along the pressure axis. So the governing assumption here is that the strong panels were at or near the onset of damage and exhibited some minor cracking on the rear face. The results of the analysis are quite sensitive to the accuracy of this assumption and the issue of result sensitivity will be discussed later.

10.1.2 Figure 47 is a summary plot which shows the onset-of-damage iso-damage curve for the strong panel when subjected to each of the assumed load types. Points to note are:

- The pressure asymptote ranges from approximately 14kPa to 18kPa for all of the load types. This is a relatively small range.
- The impulse asymptote ranges from approximately 1kPa.s to 4kPa.s. This is quite a wide range.
- It can be concluded that onset of damage to the strong panel is sensitive to the peak applied pressure and relatively insensitive to the total applied impulse.
- The assumed load shapes C and D produce almost identical iso-damage curves even though the form of these loads is significantly different.
- The iso-damage curve for the vapour cloud explosion (load A) and the HE

explosion (load B) are almost identical in the impulsive region of the pressure dependent part of the PI diagram.

- The most noteworthy feature of the response is that in the dynamic and impulsive region of the PI diagram for the vapour cloud explosion (load A) is of a different shape than for the other three assumed load forms. The pressure assymptote of the damage curve for the vapour cloud explosion is shifted upward slightly when compared to the other load types. This is a well understood phenomenon and is related to the finite rise time at the beginning of the load curve.

10.1.3 Figure 48 is a summary plot which shows the 200mm iso-damage curve for the weak panel when subjected to each of the assumed load types. Points to note are:

- Again, the pressure asymptote ranges from approximately 14kPa to 18kPa for all of the load types. This is a relatively small range.

- The impulse asymptote ranges from 2kPa.s to 10kPa.s. This is quite a large range.

- The vapour cloud explosion and the HE explosion (assumed loads A and B) produce near identical 200mm iso-damage curves for the weak panel.

- Assumed loads C and D produce near identical 200mm iso-damage curves for the weak panel.

- There is a very large difference between the response to assumed load shapes A&B and shapes C&D. This is due to the fact that shapes C&D are characterised by the inclusion of a very sharp pressure spike to represent a localised high order blast. Assumed shapes A and B only consider a "global" blast.

- The dynamic region of the PI diagram is larger for the 200mm iso-damage curve for the weak panel than the 30mm iso-damage curve for the strong panel. The dynamic region is the "elbow" region where neither peak pressure nor total impulse dominate the structural response.

10.1.4 By far the most important results plots in this whole assessment are those which show the iso-damage curves for onset of damage to the strong panel and 200mm deflection of the weak panel. The primary concept behind this study was that these two iso-damage curves would cross at a point where a single load curve produces the correct structural response for both the strong and weak panels. These plots are shown in Figure 31, Figure 36, Figure 41 and Figure 46 for assumed blast loads A, B, C and D respectively.

10.1.5 Of the four assumed load types, the only one which produces crossing iso-damage curves is the assumed vapour-cloud explosion shaped load curve. This crossing is shown in Figure 31. The feature that causes these curves to cross is the curvature of the onset-of-damage curve along the pressure asymptote. Without this feature the iso-damage curves do not cross. This feature is a result of the finite rise time associated with a vapour cloud explosion where there is no high-order detonation.

10.1.6 The conclusion to be drawn from this behaviour is that the blast loading which caused the observed damage to the Northgate cladding panels would be consistent with a large scale deflagration of a vapour cloud without any significant high-order detonation effects.

10.1.7 The iso-damage curves for the vapour cloud shaped load curve cross at a peak pressure of approximately 16.3kPa and a total impulse of approximately 11kPa.s. This crossing point represents a single pressure load curve which would cause 200mm permanent deflection of the weak cladding panels while at the same time causing only cracking with little deformation in the strong cladding panels. The actual load curve to cause this behaviour is shown in Figure 49. The total duration of this positive phase loading, including the rise time and the decay time, is approximately 1.6 seconds.

10.1.8 A general trend that is apparent in the whole result set is that smoother load curves produce responses more like those observed on-site than non-smooth load curves with sharp pressure spikes. This trend would suggest that the actual load curve which caused the damage to the Northgate cladding panels was a smooth curve rather than a curve including sharp pressure spikes. This behaviour is a result of the peak-pressure sensitive nature of the structural response. Any curve with a sharp pressure spike higher the ultimate strength of the strong panel results in a significant displacement (greater than 30mm). But a sharp pressure spike (with a short duration) would tend not to cause a significant deformation (200mm) of the weak panel. These two trends work against each other meaning that load curves with sharp pressure spikes are less likely to produce the desired structural response than smooth load curves.

10.1.9 It has been mentioned previously that the results may be sensitive to the estimated deformation level to represent onset of damage to the strong panel and failure of the weak panel (30mm and 200mm respectively). The sensitivity to these values becomes clear when examining the results from the HE shaped load curve.

10.1.10 It is unlikely that the permanent deflection of the strong panel was any more than the estimated value otherwise it would have been visible on-site and in the photographs of the damage. It could however be less than this value, particularly if the concrete did not crack. Reducing this value would not change the response to load curves B, C and D: the damage curves would still not cross and would be even further separated. Reducing this value would change the location of the crossing point on the load type A damage curves by increasing the impulse significantly without significantly changing the pressure. This is consistent with the pressure-sensitive, impulse-insensitive nature of the structure.

10.1.11 The estimate that the permanent deflection of the failed panels was around 200mm is probably quite accurate. The photograph shown in Figure 5 gives a clear view of the deformation and allows the magnitude of the deflection to be measured relative to the thickness of the panel (which is known). The size of the error in this estimate is likely to be relatively small. Additionally the spacing between the 100mm and 300mm iso-damage curves for the panels is quite small. So the results are relatively insensitive to this estimated value.

10.1.12 It is also possible that there will be some sensitivity to the estimated material properties. However, the magnitude of this sensitivity is very difficult to determine.

10.1.13 Even so, given the sensitivity of the results to all estimated data, the general trends in the

response will remain the same. The primary conclusions are still valid: a smooth pressure load curve of long duration and peak pressure around 15kPa to 20kPa is the most likely form of loading which could have caused the observed structural response. Load curves with sharp, short duration pressure spikes above these levels are unlikely to produce the observed structural response.

11. Detailed finite element analyses of selected loadcases

11.1 Selection of loadcases

11.1.1 The final Phase of this study was to conduct a relatively small number of fully dynamic finite element calculations to confirm the predictions of the single-degree-of-freedom analyses and to investigate further any loadcases of specific interest. The loadcases to be considered in these analyses were to be selected in consultation with DOSG subsequent to the delivery of an interim report.

11.1.2 The SDOF models were developed based upon a static load-deflection response calculated by FE analysis. Therefore the pseudo-static region of the response of the SDOF models would automatically produce the same response as the FE analyses. This is quite easily confirmed by comparing the pressure asymptote of the PI-diagrams to the pseudo-static failure load predicted by the FE analyses.

11.1.3 A total of 7 loadcases were selected for this set of more detailed analyses. These loadcases are listed in Table 2. For ease of reference these loadcases will be designed DLC_1 to DLC_7 (Detailed Load Case _x).

11.1.4 DLC_1 and DLC_2 are triangular load pulses with near-zero rise time. These were chosen for analysis to confirm that the SDOF models that were developed above would give similar results to the detailed FE models in the dynamic response regime as well as in the quasi-static regime were they were developed.

11.1.5 DLC_3 and DLC_4 were chosen to confirm the primary conclusion that a load curve representative of a large vapour cloud deflagration, as shown in Figure 49, would result in structural damage similar in form and magnitude to that observed on-site.

11.1.6 It has been suggested by other investigators that a condensed explosive charge equivalent to 7.5Te TNT up to 100Te TNT (depending upon which blast indicators are used) could produce similar damage levels to those observed on-site. This wide range of estimates is likely due to the fact that the loads resulting from a vapour cloud explosion (a thin large diameter disc-shaped cloud in this case) and a condensed explosive (which is essentially a point source) are dissimilar. It is widely accepted that the pressure field close to a VCE cannot be accurately represented by the load curve of an "equivalent" condensed explosive charge. This is less true at large distances from the explosion but since the Northgate panels being assessed here are within the perimeter of the vapour cloud it seems very unlikely that it would be possible to derive an appropriate equivalent TNT charge, irrespective of whether the cloud detonated or deflagrated. However, it is still informative to investigate these TNT scenarios to give an insight into the response of the panels in the high-pressure/short-duration regime where detonation is more of an issue than deflagration.

11.1.7 A total of 3 "TNT scenarios" were considered, DLC_5 up to DLC_7. The standoffs considered range from 50m to 135m from the façade which puts the charge somewhere towards the centre of the cloud. Again it has to be emphasised that a TNT charge at the centre of the cloud is never likely to give the same pressure field as would exist at the edge of a large VCE irrespective of whether if detonated or deflagrated.

Applied load	*Peak pressure (kPa)*	*Total Impulse (kPa.s)*	*Total duration (msec)*	*Weak-or-strong panel*	*t_d/T*	*Reference (Detailed Load Case x)*
Triangular load:	17.5	7.5	857	Weak	12.2	DLC_1
Triangular load:	20.0	3.0	300	Weak	4.2	DLC_2
VCE at crossing point of iso-damage curves	16.3	11.0	1600	Strong	22.8	DLC_3
VCE at crossing point of iso-damage curves	16.3	11.0	1600	Weak	22.8	DLC_4
7.5Te **TNT** @ 135m	56.1	1.7	61.7	strong	0.88	DLC_5
7.5Te **TNT** @ 135m (triangular)	56.1	1.7	61.7	weak	0.88	DLC_6
7.5Te **TNT** @ 50m (triangular)	515.1	5.3	21.0	weak	0.3	DLC_7

Table 2; List of loadcases for detailed FE analysis.

11.2 Results: DLC_1 and DLC_2

11.2.1 These two loadcases were selected from the PI diagrams developed from the SDOF analysis. The points were chosen to be within the "bend" of the PI diagram which represents the region where neither peak-pressure nor total-impulse dominates the structural response and to be within the moderate damage region. These loadcases were chosen to confirm that the SDOF models were valid near the dynamic regime.

11.2.2 It is difficult to define in general terms where the quasi-static, dynamic and impulsive regions begin and end for a particular structure. However, it is quite common to use the ratio between the duration of loading and the natural period of the structure as a measure of which response regime the structure is likely to be in. Table 3 lists typical limits for these response regimes. It should be borne in mind that these limits are only typical values and will vary depending on the structure and the loading considered but they will be used here as indicative values.

Impulsive	$t_d/T < 0.2/\pi$
Dynamic	$0.2/\pi < t_d/T < 20/\pi$
Quasi-static	$t_d/T > 20/\pi$

Table 3; Typical delimiters of three response regimes in terms of load-duration/natural period of structure [5].

11.2.3 DLC_1 with a t_d/T ratio of 12.2 is in the impulsive region and DLC_2 with a t_d/T ratio of 4.2 is in the dynamic regime according to the indicative levels given in Table 3. Figure 50 shows the iso-damage curves for a triangular load applied to the weak panel with two points marked to indicate the position of DLC_1 and DLC_2 on these curves. Clearly both of these load cases are in the dynamic part of the curve.

11.2.4 Figure 51 and Figure 52 show front and rear views of the damaged "weak" panel finite element model resulting from DLC_1. The permanent deflection and failure mode are quite difficult to discern from these views but the primary mode of failure is through yielding of the rebar around midspan of the beam sections of the panel. However, there is no clearly delineated fracture down the middle of the panel as was visible on-site.

11.2.5 A more useful plot is shown in Figure 53 which presents the displacement-vs-time response of the panel to DLC_1 and DLC_2. The initial elastic part of the response is similarly predicted by both SDOF and FE models. The elastic unloading slope is less well predicted by the SDOF models due to the fact that the unloading stiffness was assumed to be the same as the loading stiffness. However, the permanent deflection predicted by the SDOF models is quite close to that predicted by the FE models. DLC_2 results in a permanent deflection of 129mm which compares to 119mm predicted using the SDOF model. DLC_1 results in a permanent deflection of 190mm and 229mm according to the SDOF and FE models respectively. The conclusion is that the SDOF models predict the response in the dynamic regime within around 20%.

11.2.6 It should be remembered that the SDOF models are very simple models and will never be able to full represent the whole complex behaviour of a structure. However, if these simple models can predict the structural response to within 20% in the dynamic regime and to within almost 0% in the quasi-static (due to the SDOF models being defined by the response in this region), then they can be used with some degree of confidence to predict the structure response to a wide range of loading types and magnitudes.

11.2.7 A very important point to note here is that the further into the impulsive regime that a particular load curve is, the more complex the failure mode. In the quasistatic regime the failure mode is a pure flexural failure with a single vertical crack down the centre of the panel. In the dynamic regime the failure mode tends to be more distributed with several cracks forming on the back face of the panel. In the impulsive regime this is even more obvious as will be illustrated in later examples.

11.2.8 The coarse version of the finite element model was used for DLC_1 to DLC_4 because these loadcases were within the region where simple flexural behaviour was dominant. DLC_5 to DLC_7 were all in the region where a more complex failure mode would be expected so these were analysed using a much higher resolution finite element model.

11.3 Results: DLC_3 and DLC_4

11.3.1 These two loadcases represent the scenario that the SDOF models predicted would result in structural behaviour similar to that observed on-site. The applied load curve is the same for DLC_3 and DLC_4 which are for the strong and weak panels respectively. The applied load curve is a smooth curve with a finite rise time and a long decay. This is a low intensity / long duration load representative of a vapour cloud deflagration.

11.3.2 Figure 54 shows a view of the damage to the rear of the weak panel after DLC_3. In this view there is a very well defined crack visible which runs vertically near midspan of the panel. This matches closely with what was observed on site.

11.3.3 Figure 54 can be compared directly with Figure 52 to illustrate the difference in failure mode in the quasi-static and dynamic/impulsive regimes.

11.3.4 Figure 55 shows deflection-vs-time curves for DLC_3 and DLC_4.

11.3.5 The first feature to note on this plot is that the trends predicted by the FE and SDOF models are very similar but that the FE models predict generally higher permanent deflections. This is likely due to the sensitivity of these results to the load duration as has been explained previously. The trend shown by both models is that for this type of loading there is a significant difference in response of the two panels.

11.3.6 The primary feature of interest from this plot is this difference between the response of the weak and strong panels. The difference in permanent deflection is about 200mm. This is similar to what was observed on-site. The difference in response is much greater than would be expected from the slight difference in strength of the two panels and is influenced as much by the form of the loading as by the structural differences.

11.3.7 It is important to note that the only form of loading that has been found to produce both the correct failure mode, a single vertical fracture at midspan, and a significant difference in response of the two panels is the load curve representing a low pressure but long duration explosion with a finite rise-time.

11.3.8 It can be concluded that the finite element models generally confirm the conclusions drawn from the SDOF analyses except that the blast load duration is indicated to be a little shorter than suggested by the SDOF models. As a rough estimate, based upon the finite element analyses, a load duration closer to 1.2 seconds would be more accurate, instead of the 1.6 seconds suggested by the SDOF models.

11.4 Results: DLC_5, DLC_6 and DLC_7

11.4.1 These loadcases represent "TNT equivalent" scenarios. It has been explained previously that TNT and vapour clouds produce very different pressure fields close to the explosion and that a TNT equivalency for the Northgate panels would not be entirely appropriate.

11.4.2 Figure 56 shows the deflection-vs-time responses for the weak and strong panels in DLC_5 and DLC_6.

11.4.3 The first thing to note from this plot is that the magnitude of the permanent deflection is of a similar order to that observed on-site. Both panels were moderately damaged by the 7500kgTNT@135m scenario. However, both panels respond in essentially the same way without the large difference in response that was observed on-site. Comparing Figure 56 directly with Figure 55, which shows a similar plot for the VCE loadcases, the difference in the form of the response is clear.

11.4.4 Equally important is the predicted failure mode. Figure 57 shows the damage to the rear of the weak panel for the 7500kgTNT@135m loadcase. It is immediately obvious that the failure mode involves three primary cracks on the back face of the panel. This occurs due to the significance of the shear behaviour of the panel relative to the flexural behaviour. With loadcases involving higher peak pressures the influence of the shear behaviour increases. When the shear behaviour is dominant there would not be a single well defined crack at midspan on the panel. There is also a loading range where there are combined shear and flexural effects and where damage at midspan is of a mixed mode. The 7500kgTNT@135m scenario is within this range as illustrated by the failure mode shown

in Figure 57.

11.4.5 DLC_7 was chosen to be at the impulsive end of the dynamic response regime. This loadcase is equivalent to 7500kg of TNT at a standoff of 50m. The peak pressure in this scenario was 515.1kPa (which is approximately 5bar *reflected* pressure). This is of the same order of magnitude as the pressures that would be experienced inside, or near to the edge of, a detonating vapour cloud where pressures of several bar could be expected. A large detonating vapour cloud producing this level of pressure would produce a significantly longer load duration than is produced by the TNT charge and would result in more severe damage to structures.

11.4.6 Even so, DLC_7 causes severe damage to the Northgate panels. Due to the impulsive nature of the loading and the structural response it is necessary to view the failure mode as it progresses through time. Figure 58 shows a series of images taken at 20msec intervals during DLC_7. From these images it can be seen that failure initiates at the ends of the panel near the supports. This is shear dominated response. As time progresses the damage gradually spreads towards the centre of the panel in a series of vertical cracks. The deformed panel takes the shape of a continuous curve rather than having a single sharp bend at midspan as was observed on-site. There is also evidence of a horizontal crack forming along the full length of the panel.

11.4.7 It seems likely that a large vapour cloud detonation capable of producing peak reflected pressures of several bar would have completely destroyed the Northgate cladding panels instead of just causing moderate/heavy damage with a single midspan crack. It also seems likely that such and event would result in a completely different failure mode than was observed on-site.

12. Sensitivity to material properties

12.1.1 It is always the case with the type of assessment conducted here that some important information about the structure is unknown. In this case the largest uncertainty is with the properties of the materials used in the construction of the panels.

12.1.2 The strength of the concrete does not have a large influence on the response because the behaviour is dominated by yielding of the reinforcement. This is normally the case because reinforced concrete is designed to be under-reinforced such that the reinforcement yields before the concrete crushes. This is usually a design requirement and it is intended to ensure the structure is ductile rather than brittle.

12.1.3 The mechanical properties of the reinforcing steel were unknown at the time this analysis was conducted. In the absence of this data typical design values were used. The actual strength of the reinforcement is usually stronger than the specified minimum strength used for design purposes. However, it would have been difficult to justify using arbitrarily higher strength values for the steel without validating evidence.

12.1.4 However, subsequent material tests have shown that the reinforcement steel could be significantly stronger than the design values used in the initial assessment, with tensile strengths up to around 600MPa.

12.1.5 It is obvious that the increase in strength of the panel that would result from the increased strength of the reinforcing steel would influence the results of this study. A simple estimate would suggest that using a 600MPa yield stress for the steel would increase the strength of the panels by around 30%. It can be envisaged that there would be a similar increase in the magnitude of the pressure loading that would be required to cause the observed damage to the Northgate panels. However, it could also be envisaged that the general form and order of magnitude of the results would not change.

12.1.6 This estimated 30% variation in the strength of the panels due to uncertainty regarding the material properties can be compared to the difference between the pressures associated with a deflagration and detonation of a vapour cloud. There can be two orders of magnitude difference between deflagration and detonation pressures.

12.1.7 Based upon this reasoning it seems unlikely that uncertainty in the strength of materials would alter the conclusion that the blast which caused the damage to the Northgate panels was more likely to be a deflagration than a detonation.

12.1.8 In order to confirm that panels with an increased strength reinforcing steel would still respond as expected to a long-duration-low-pressure loading, a further batch of SDOF analyses were conducted. This time the SDOF models were treated as elastic-ideally-plastic with the ultimate strength chosen to be 30% higher than was initially estimated for the panels.

12.1.9 Figure 59 shows the end result of this additional set of SDOF analyses in terms of crossing iso-damage curves for 30mm permanent deflection of the strong panel and 200mm permanent deflection of the weak panel. The crossing point for these strengthened panels occurs at a peak pressure of 29kPa and a total impulse of 7.5kPa.s. The resulting load curve is shown in Figure 60 alongside the original estimate which used the design material properties.

12.1.10 Since the Northgate panels were within only a few meters of the edge of the vapour cloud it seems unlikely that a detonation would be able to produce loads of this form and magnitude. Accounting for a very wide range of possible material strengths it is predicted that a smooth load curve with a peak pressure between 15kPa and 30kPa, and a duration between 1.6 and 0.6 seconds would be capable of producing the damaged observed on-site.

13. Conclusions

13.1.1 The primary conclusions of this assessment are:

- The responses of the reinforced concrete cladding panels used on the Northgate building are sensitive to the magnitude of the peak applied pressure and relatively insensitive to the applied impulse within the regimes considered.

- Pressure load curves which include relatively short duration, high intensity pressure spikes are unlikely to produce significantly different responses of the weak and strong cladding panels. The difference in the response of the weak and strong panels

tends to discount the possibility that there were high-order detonation effects, of a scale large enough to affect the whole Northgate building façade, involved in the Buncefield explosion.

- It has been shown that a smooth blast loading curve with a finite rise time and exponential decay, with the rise time being 30% of the overall duration and the decay being 70% of the overall duration, with a peak pressure of 15kPa to 30kPa and a duration between 1.6s and 0.6s respectively would produce the actual structural deformation observed on-site.

13.1.2 It is evident that the results presented above can be quite sensitive to some of the assumptions that had to be made regarding the structural definition of the panels, the properties of the materials used in the construction of the panels and the actual structural response. However, it has been concluded that the general trend of the results would not change significantly and that the primary conclusions presented above are valid.

13.1.3 Although the precision of the results is affected by uncertainty regarding material properties it is evident that the end results all lie within the low-pressure-long-duration regime rather than in the high-pressure-short-duration regime. This is not conclusive evidence that there were no high-order detonation effects involved in the Buncefield VCE but it is a good indication that there was not a large scale detonation.

13.1.4 It has been shown that hand-calculations, finite element analyses and single-degree-of-freedom analyses produce consistent results. This gives a degree of confidence that the results are valid and accurate within the bounds of the stated assumptions.

13.1.5 A total of 200,000 loadcases were analysed for each panel type in this study. If the results of CFD analyses conducted by other investigators were available then it would be a relatively straightforward exercise to assess the structural response to specific load curves using the SDOF models developed here.

14. References

14.1 General references

1. Comite Euro-International Du Beton, "CEB-FIP MODEL CODE 1990", Thomas Telford, June 1993.
2. Baker W E *et al*, "*Explosions hazards and evaluation", Elsevier 1983.*
3. Smith P D and Hetherington J G, "*Blast and Balistic Loading of Structures*", Butterworth Heinemann Ltd, 1994.
4. Smith P D and Cormie D, "*Blast Effects on Buildings 2nd Edition: Chapter 5: Structural Response to Blast*", Unpublished draft 2009.
5. Weidlinger Associates Ltd, "*Explosive store house break-up modelling: Single leaf and cavity wall trials – pre-trial modelling*", Weidlinger Associates Ltd., Ref. DES07021_080310_AN_V1.0, 28 Match 2008.

14.2 FLEX related supporting references

6. Vaughan, D. K., "*FLEX User's Guide*," Report UG8298, Weidlinger Associates, Los Altos, CA, May 1983 plus updates through 2006.
7. Mould, J. C., Jr. and H. S. Levine (1993), "*A Rate-Dependent Three Invariant Softening Model for Concrete*," published in Studies in Applied Mech., Mech. and Materials and Structures, Ed. by G.Voyiadjis, L. Bank and L. Jacobs, Elsevier, 1994.
8. DiMaggio, F. L. and Sandler, I.S., "*Material Models for Granular Soils*", J. Eng. Mech Div, ASCE V 97, No. EM3, June 1971.
9. Tennant, D., H. Levine and J. Mould, "*Prediction of Static and Dynamic Response of Reinforced Concrete Slabs Through Failure Using a Rate-Dependent Three Invariant Softening Model for Concrete*," Proc. of the 8th Internat. Symp. On Interaction of the Effects of Munitions with Structures, McLean, VA, April 21-25, 1997.
10. Mould, J., Jr., H. Levine and D. Tennant (1994), "*Evaluation of a Rate-Dependent Three Invariant Softening Model for Concrete*," Fracture and Damage in Quasibrittle Structures, edited by Z.P. Bazant, Z. Bittnar, M. Jirasek and J. Mazars, E & FN Spon, Chapman and Hall, London, UK, 1994, pp. 231.
11. Mould, J. C. and H. S. Levine (1987), "A *Three-Invariant Viscoplastic Concrete Model*", Constit. Laws for Eng. Materials: Theory and Applic., Volume I, ed. C. S. Desai, et al, Elsevier Pub. Co., Jan. 5-8, 1987, pp. 707.
12. Levine, H. S. (1982), "*A Two-Surface Plastic and Microcracking Model for Plain Concrete*," Nonlinear Numerical Analysis of Reinforced Concrete, Proc. Winter Annual Meeting, ASME, Phoenix, AZ, Nov. 1982.
13. Levine, H. S., D. Tennant and F. Wong, "*Response of Buried Vertical Steel Cylinders to High Intensity Airblast Loadings*," Proc. 1991 ASME-PVP Conference, Symp. on Structural Dynamics Produced by Extreme Loading Conditions, San Diego, CA, June 23-27, 1991.
14. Levine, H. S. and D. Tennant, "*Dynamic Buckling of Buried Steel Cylinders*," Proc. 1991 ASME Winter Annual Mtg, Symp. on Dynamic Response of Structures to High Energy Excitations, AMD-Vol. 127/PVP-Vol. 225, Atlanta, GA, Dec. 1-6, 1991.
15. Tennant, D. W. and H. S. Levine, "*Response and Failure of Internal Structural Subsystems Under Blast and Shock Loading*," ASME J. Pressure Vessel Technology, Vol. 116, No. 4, Nov. 1994.
16. Tennant, D. and H. Levine, "*Response of Embedded Cylindrical and Articulated Structures to Airblast and Ground Shock Loads*," Proc. 62nd Shock and Vibration Symposium, Springfield, VA, October 29-31, 1991.
17. Tennant, D. and H. Levine, "*Response Predictions of Reinforced Concrete Structures Subjected to Combined Airblast and Fragment Loadings*," Proceedings of the 68th Shock and Vibration Symposium, Hunts Valley, MD, November 3-6, 1997.
18. Tennant D., H. S. Levine, and J. C. Mould, Jr., "*Prediction of Static and Dynamic Response of Reinforced Concrete Slabs using a Rate-Dependent Three Invariant Softening Model for Concrete*," Proceedings of the 8th International Symposium on the Interaction of the Effects of Munitions with Structures, April 22-25, 1997.
19. Wong, F., et al, "*Tunnel Size Effects*," DSWA-TR-91-19, October 1991.
20. Wong, F., et al, "*Analytical Support to Underground Technology Program (UTP) and Lethality Assessment of Buried Structures Program*," DSWA-TR-94-189, October 1995.
21. Nikodym, L., M. Xie, F. Wong and H. Levine, "*Validation of Jointed Rock Models for Dynamic Response of Tunnels*," presented at Joint ASME, ASCE, SES Summer Annual Mtg, Northwestern U., June 29-July2, 1997.
22. Tennant, D.W., J. S. Mould, Jr., H.S. Levine, and D. K. Vaughan, "*Comparison of Crash Computations Using different Constitutive Relations for Validation of Aircraft Crash Models*,"

Proceedings 1996 Pressure Vessels and Piping Conference, PVP-Vol. 325, Structures Under Extreme Loading, July 1996.
23. Lawver, D., D. Tennant, J. Mould, Jr. and H. Levine, "*Impact of Aircraft Engines into Reinforced Concrete Walls*,' presented at the ASME Winter Annual Meeting IMECE '97, November, 1997.
24. Tennant, D., H. Levine, D. Lawver and R. Smilowitz, "*Analysis of a Multi-Story Flat Slab Building Subjected to an External Detonation Using a First Principles Finite Element Code*," Accepted for presentation at the 70th Shock and Vibration Symposium, Abuquerque, NM November 15-19, 1999.
25. Harding, D. C., et al, "Impact *Testing of the H1224A Shipping/Storage Container*", SAND94-0308, Sandia National Laboratories, Albuquerque, NM, May 1994.
26. Uncapher, W. L., et al, "*Lateral Impact Testing of a C-141B Aircraft Fuselage Section*," Sandia National Laboratories Report SAND94-2602, TT1353,October, 1994.
27. Uncapher, W. L., et al, "*Axial Impact Testing of a C-141B Aircraft Fuselage Section with Shipping Containers*," Sandia National Laboratories Report SAND94-2739, TT1360, December, 1994.
28. Heffelfinger, S., T. Blanchat and T. O'Hern, "*Test Report, TF-30 Jet Engine Impact into a Concrete Target*", Sandia National Laboratories Report, Department 9761, June 1997.

15. Figures

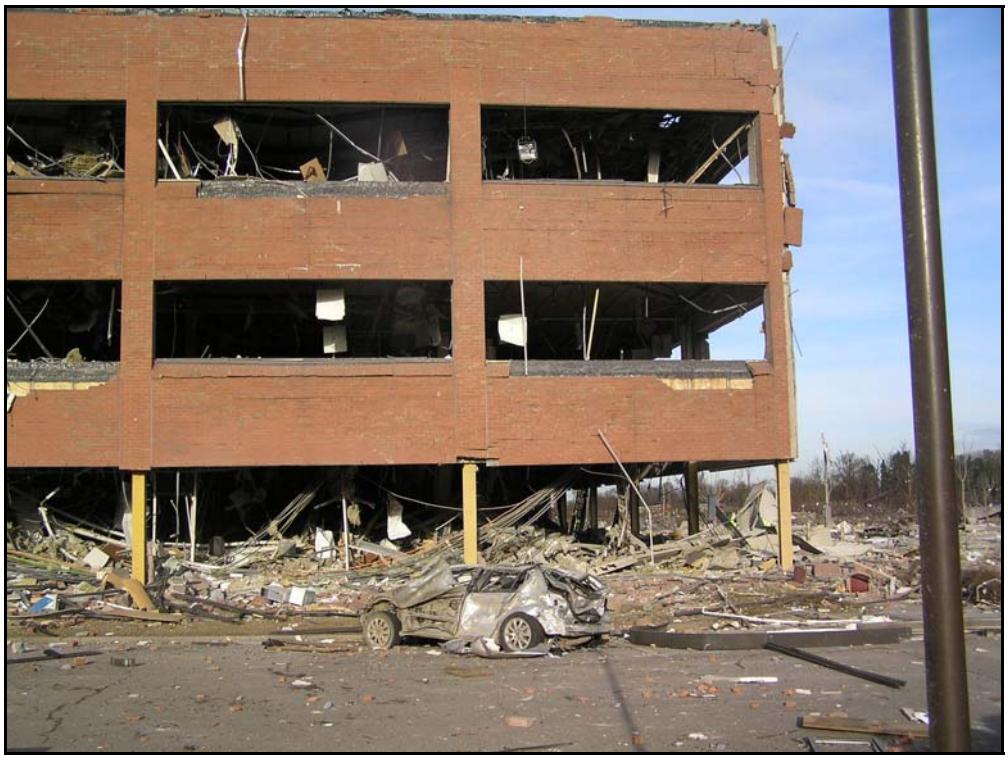

Figure 1; View of blast damage to Northgate building showing cladding panels with facing masonry still attached.

Figure 2; View of blast damage to Northgate building showing cladding panels with facing masonry removed.

Figure 3; View of blast damage to Northgate building showing detached cladding panel and connection details.

Figure 4; View of blast damage to Northgate building showing "strong" cladding panels on the left and "weak" cladding panels on the right.

Figure 5; View of blast damage to Northgate building showing permanent deflection and failure mode of "failed" cladding panel (masonry wall ties are also visible).

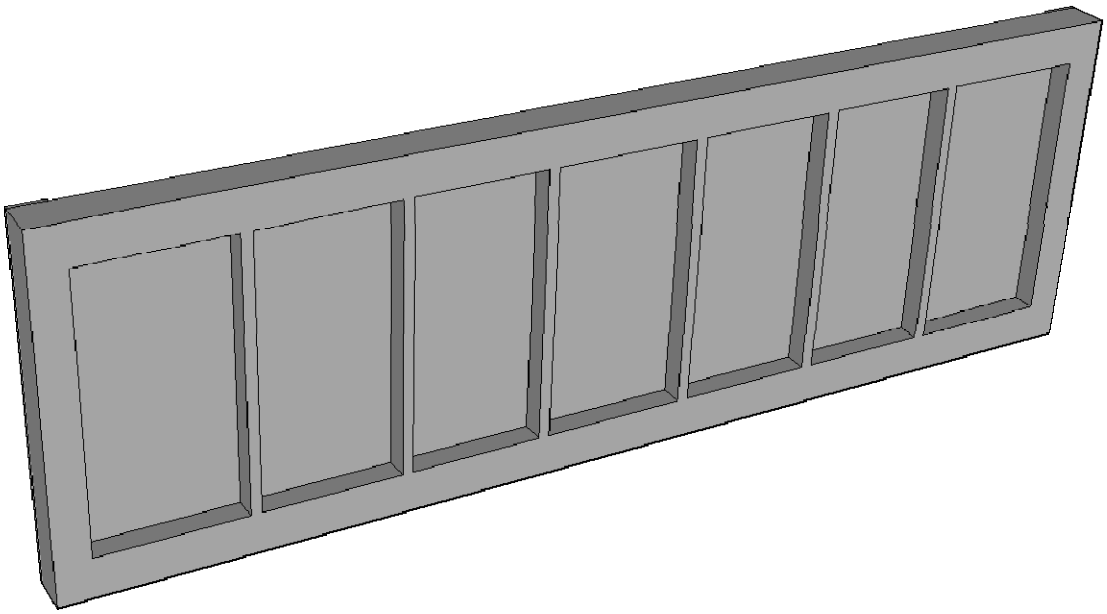

Figure 6; NL FLEX finite element model of RC cladding panel and facing masonry, fine mesh discretisation, geometry view of concrete only.

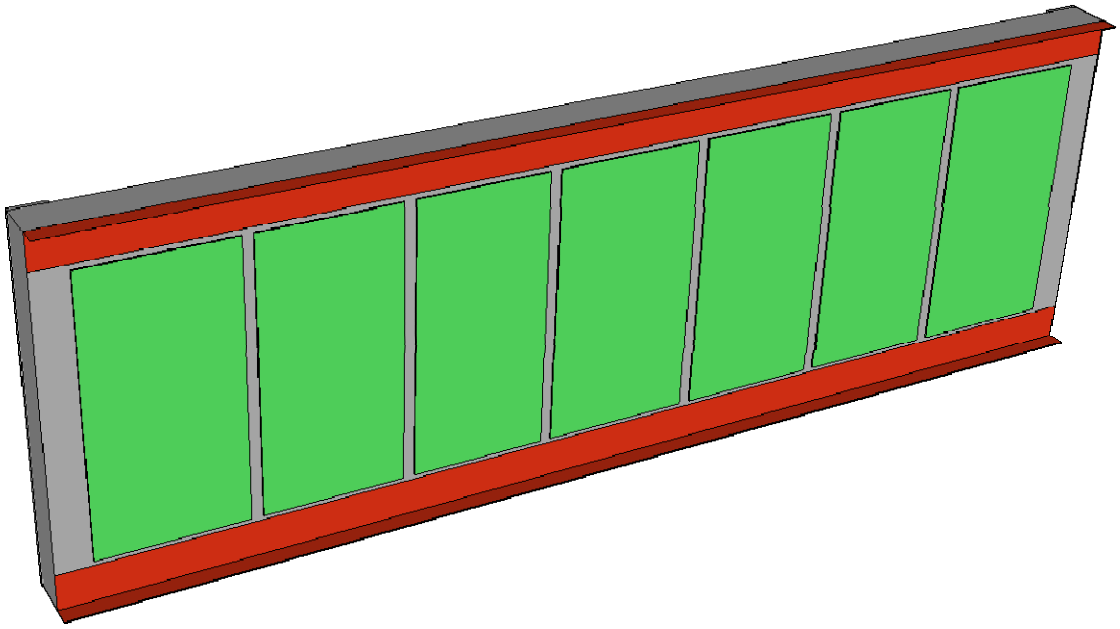

Figure 7; NL FLEX finite element model of RC cladding panel and facing masonry, fine mesh discretisation, geometry view excluding masonry.

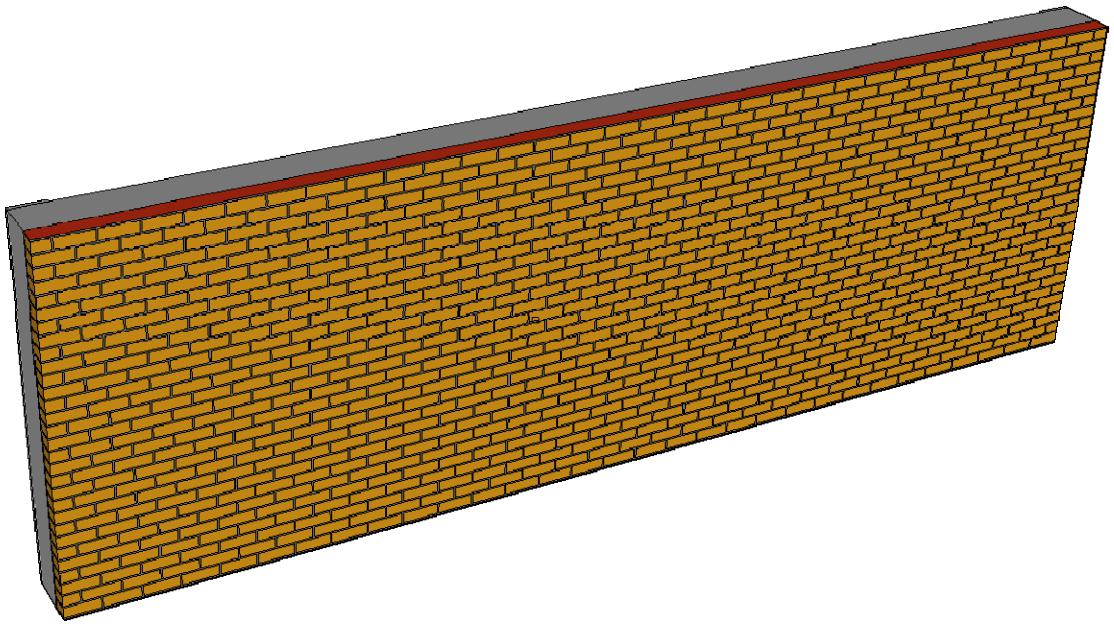

Figure 8; NL FLEX finite element model of RC cladding panel and facing masonry, fine mesh discretisation, geometry view.

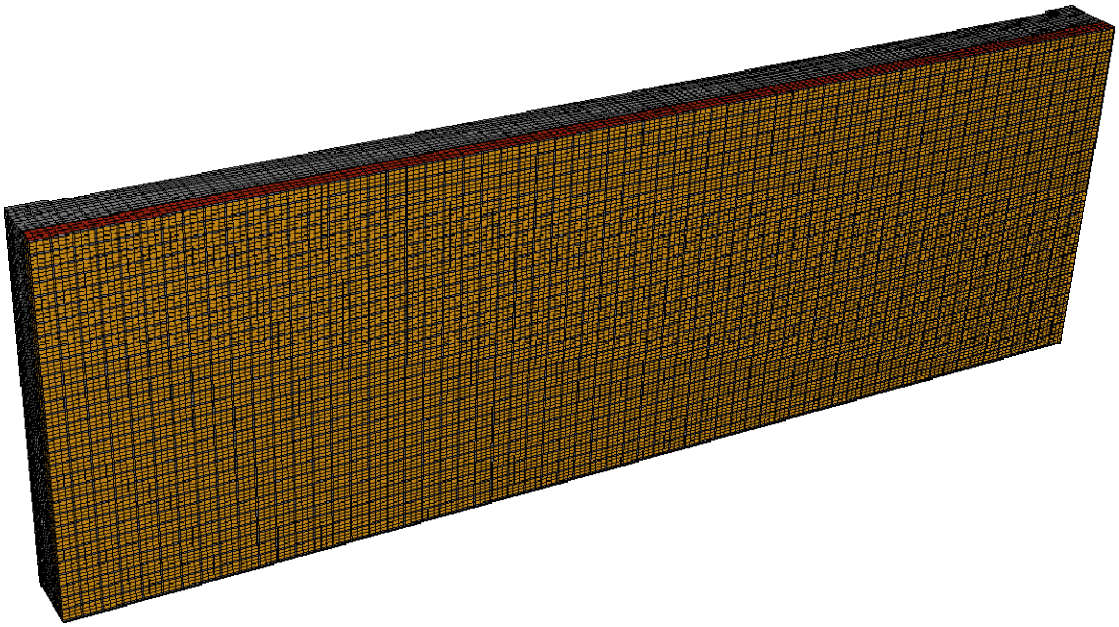

Figure 9; NL FLEX finite element model of RC cladding panel and facing masonry, fine mesh discretisation, mesh view.

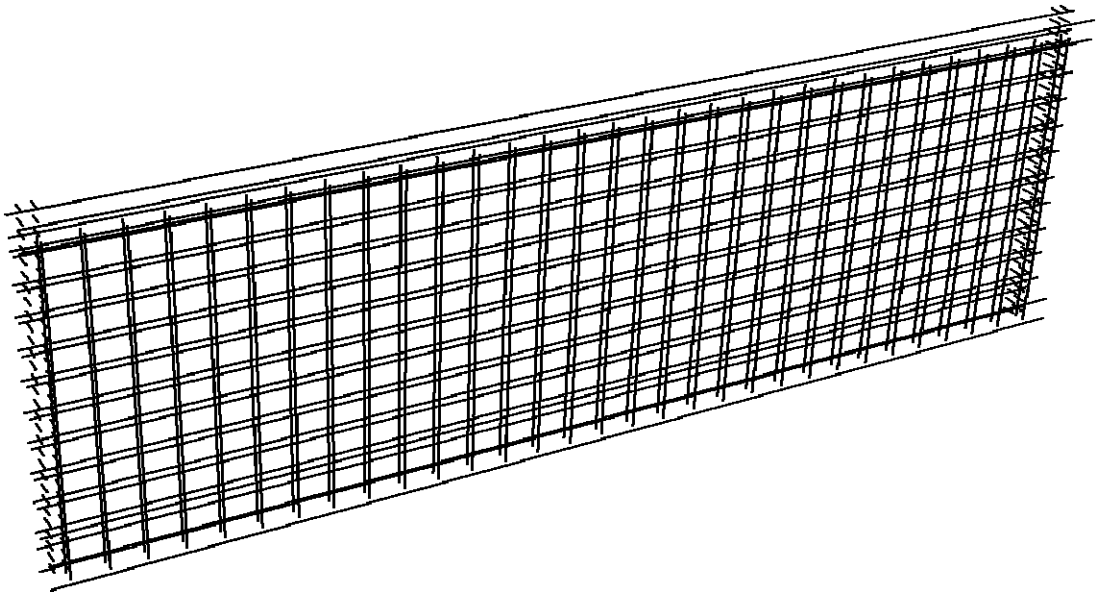

Figure 10; NL FLEX finite element model of RC cladding panel and facing masonry, fine mesh discretisation, mesh view showing reinforcement only.

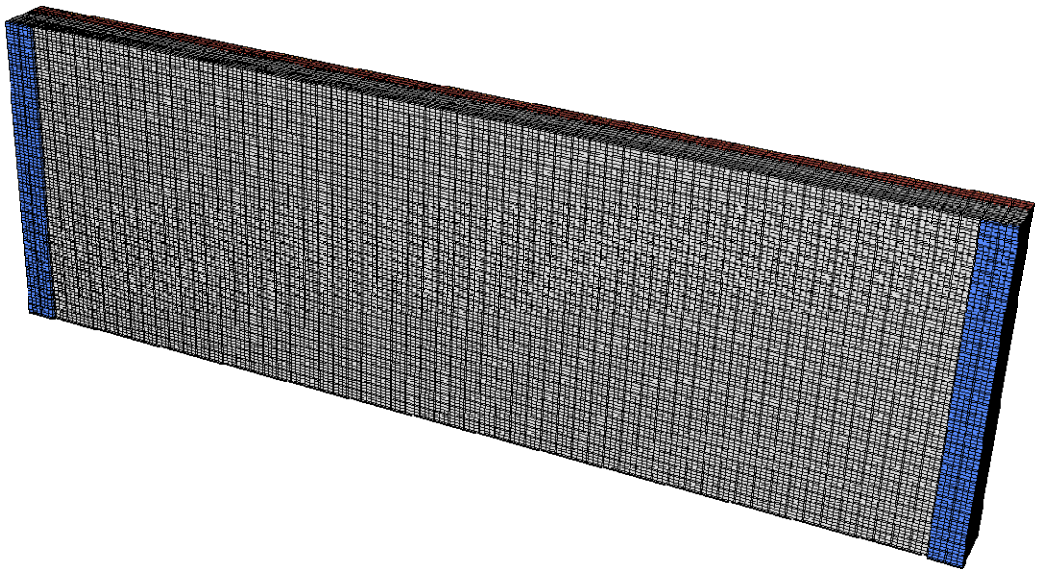

Figure 11; NL FLEX finite element model of RC cladding panel and facing masonry, fine mesh discretisation, mesh view, view or rear face showing (in blue) the end bearing pads.

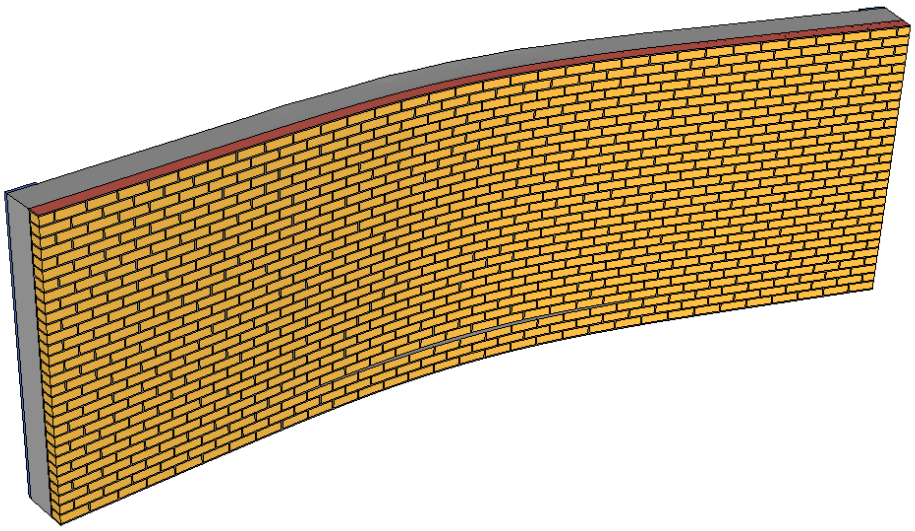

Figure 12; NL FLEX finite element model of RC cladding panel and facing masonry, fine mesh discretisation, geometry view, deformed shape of "weak" panel during test run using 100 Tonnes TNT @ 300m.

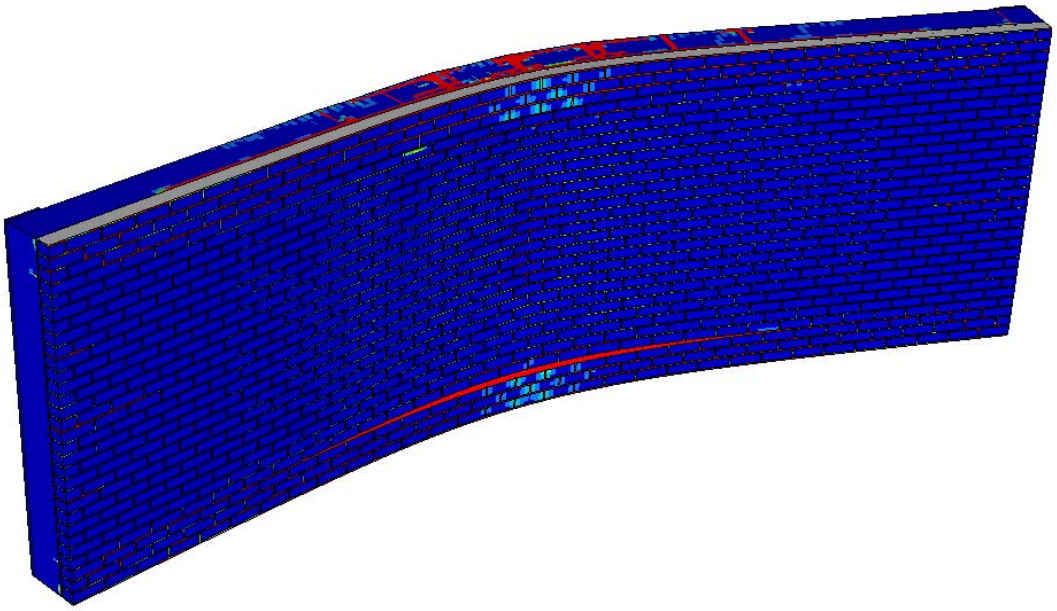

Figure 13; NL FLEX finite element model of RC cladding panel and facing masonry, fine mesh discretisation, geometry view, deformed shape of "weak" panel during test run using 100 Tonnes TNT @ 300m, contours of volumetric damage.

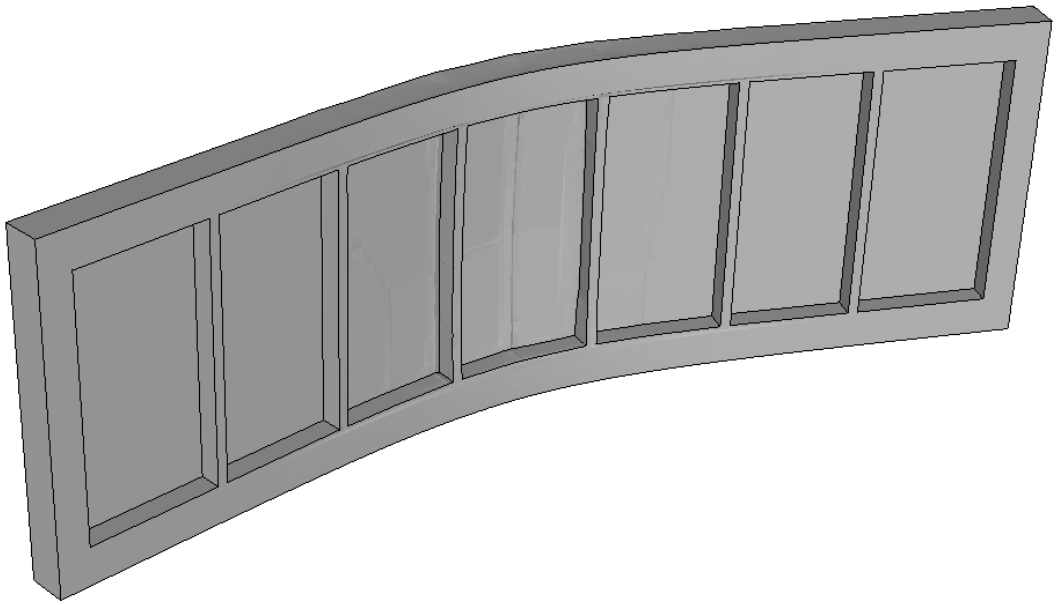

Figure 14; NL FLEX finite element model of RC cladding panel and facing masonry, fine mesh discretisation, geometry view, deformed shape of "weak" panel during test run using 100 Tonnes TNT @ 300m, showing concrete only.

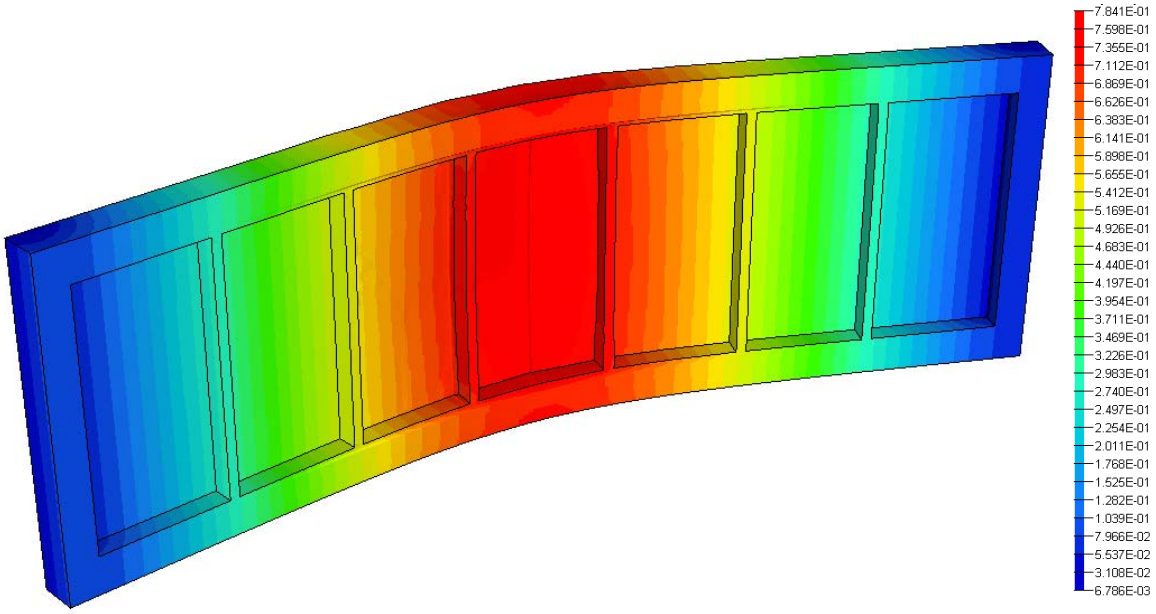

Figure 15; NL FLEX finite element model of RC cladding panel and facing masonry, fine mesh discretisation, geometry view, deformed shape of "weak" panel during test run using 100 Tonnes TNT @ 300m, showing concrete only, contours of displacement.

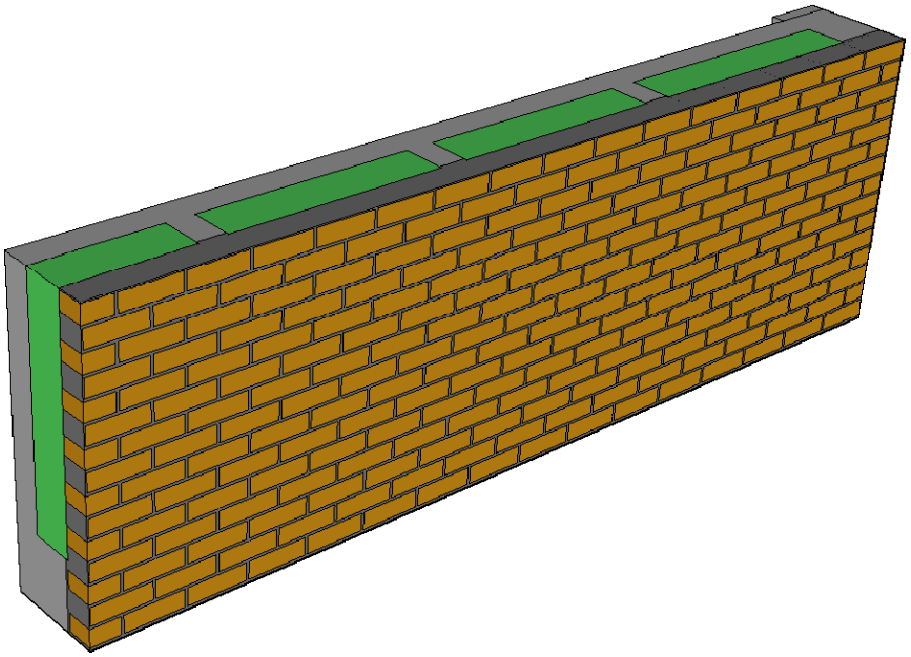

Figure 16; NL FLEX finite element model of RC cladding panel and facing masonry, coarse mesh discretisation, quarter symmetric model, geometry view.

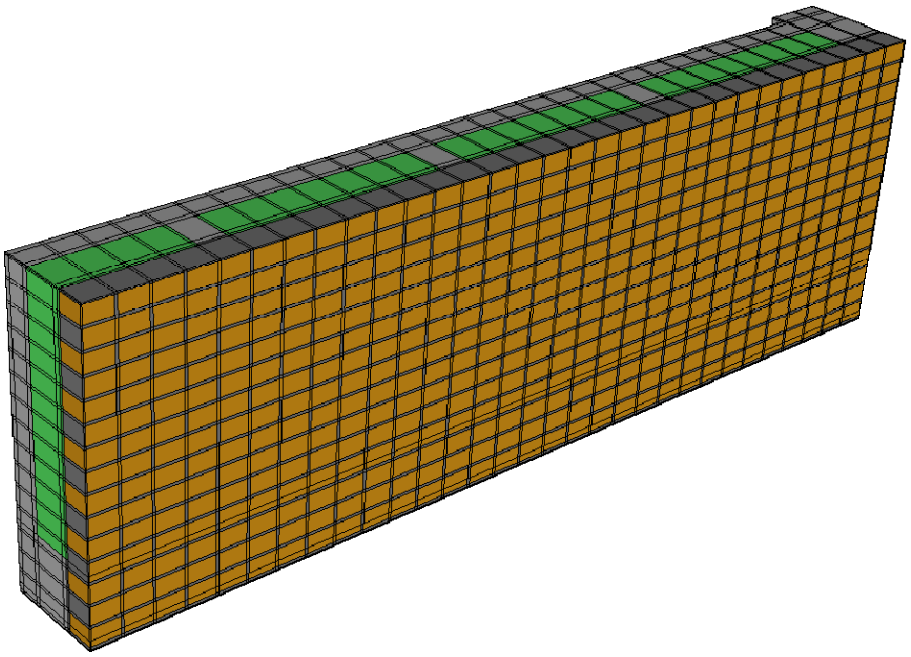

Figure 17; NL FLEX finite element model of RC cladding panel and facing masonry, coarse mesh discretisation, quarter symmetric model, mesh view.

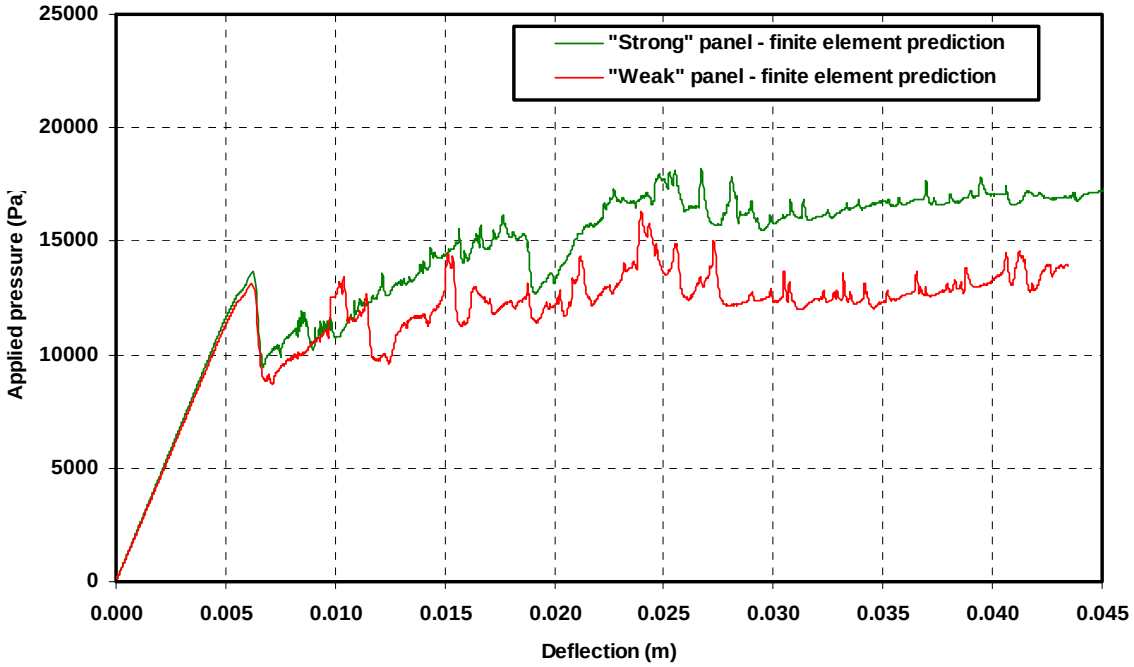

Figure 18; Pressure-deflection curves resulting from pseudo-static finite element analysis of "weak" and "strong" RC panels.

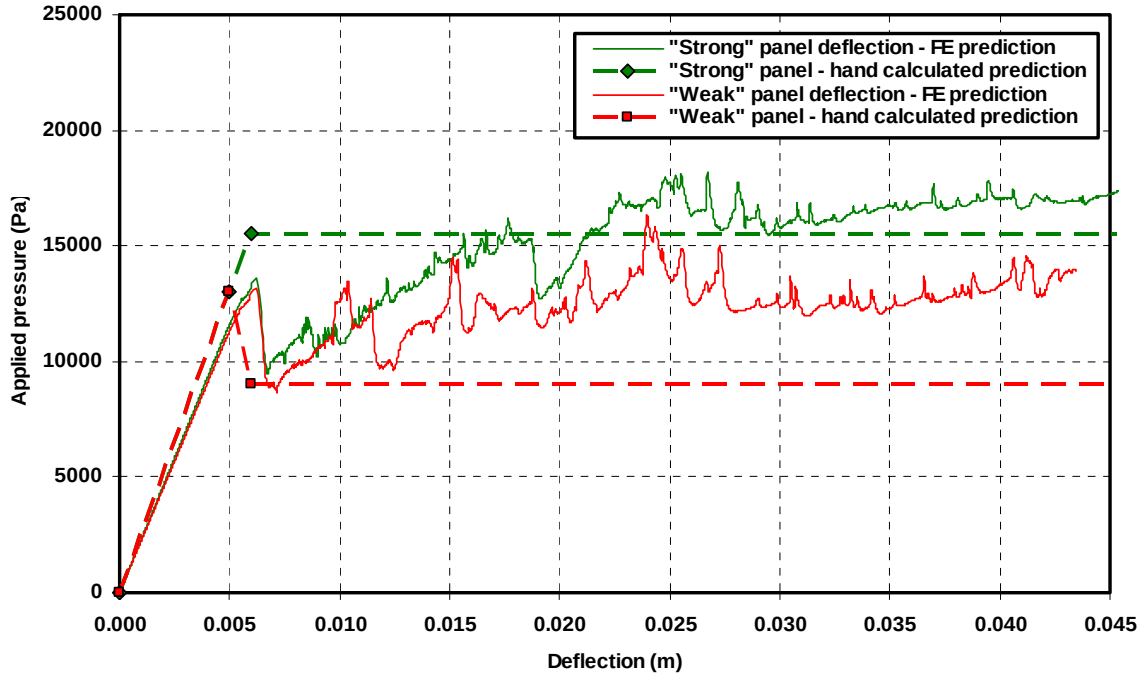

Figure 19; Pressure-deflection curves resulting from pseudo-static finite element analysis of "weak" and "strong" RC panels, with hand-calculated predictions also shown.

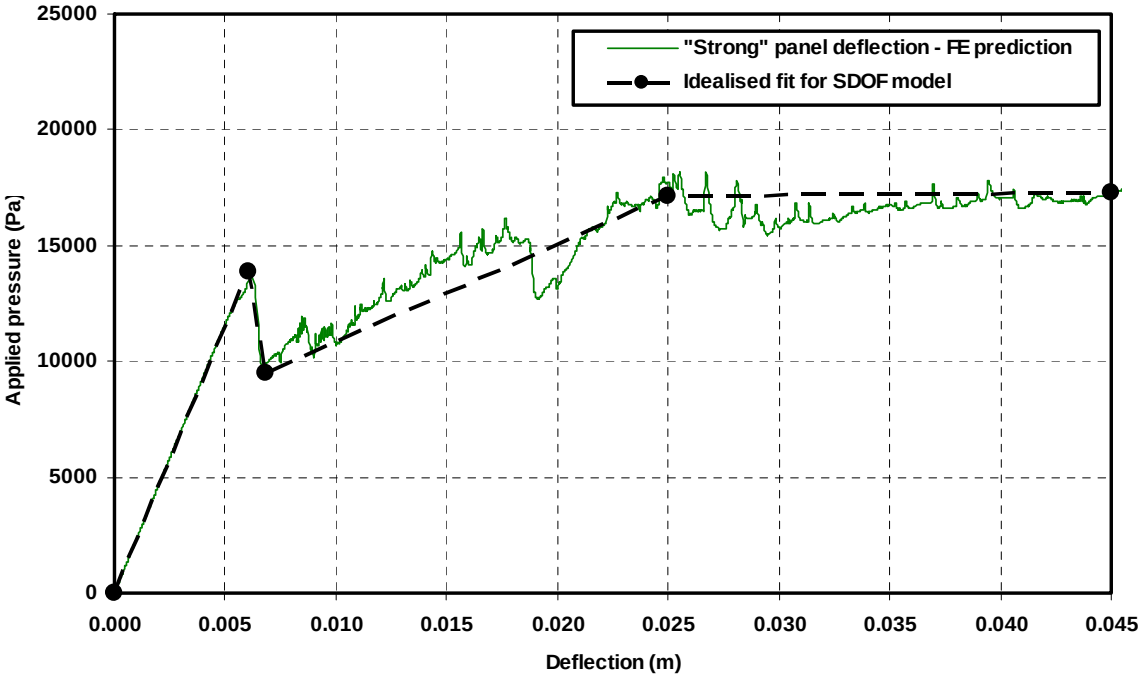

Figure 20; Pressure-deflection curves resulting from pseudo-static finite element analysis of "strong" RC panel, with idealised fit also shown.

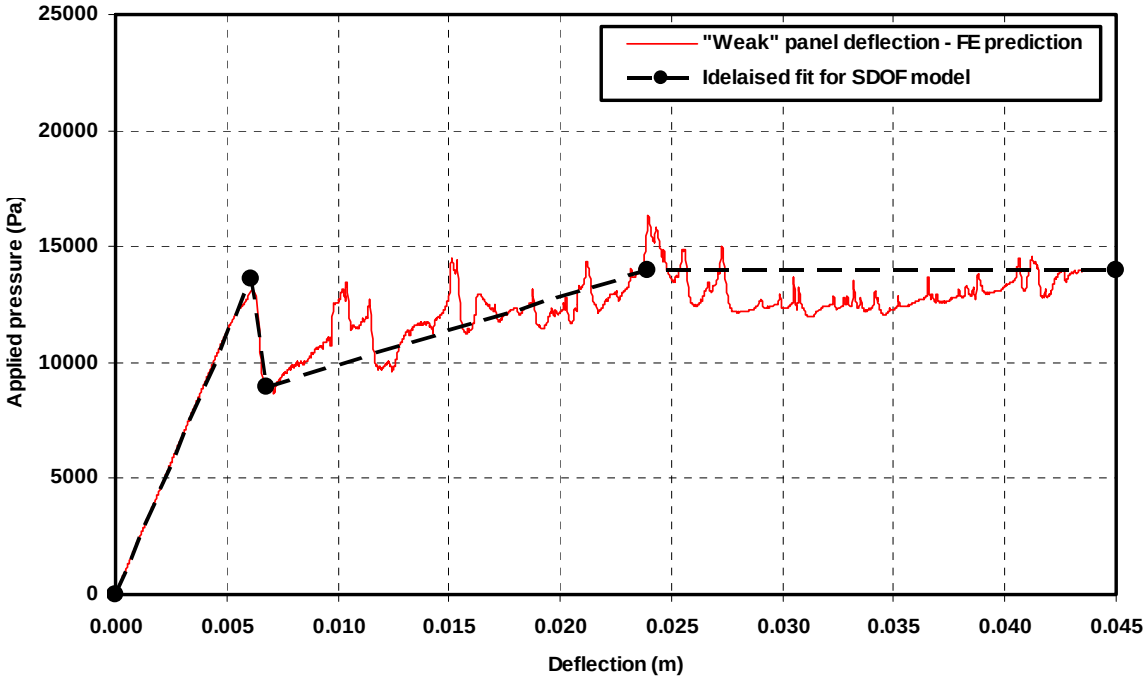

Figure 21; Pressure-deflection curves resulting from pseudo-static finite element analysis of "weak" RC panel, with idealised fit also shown.

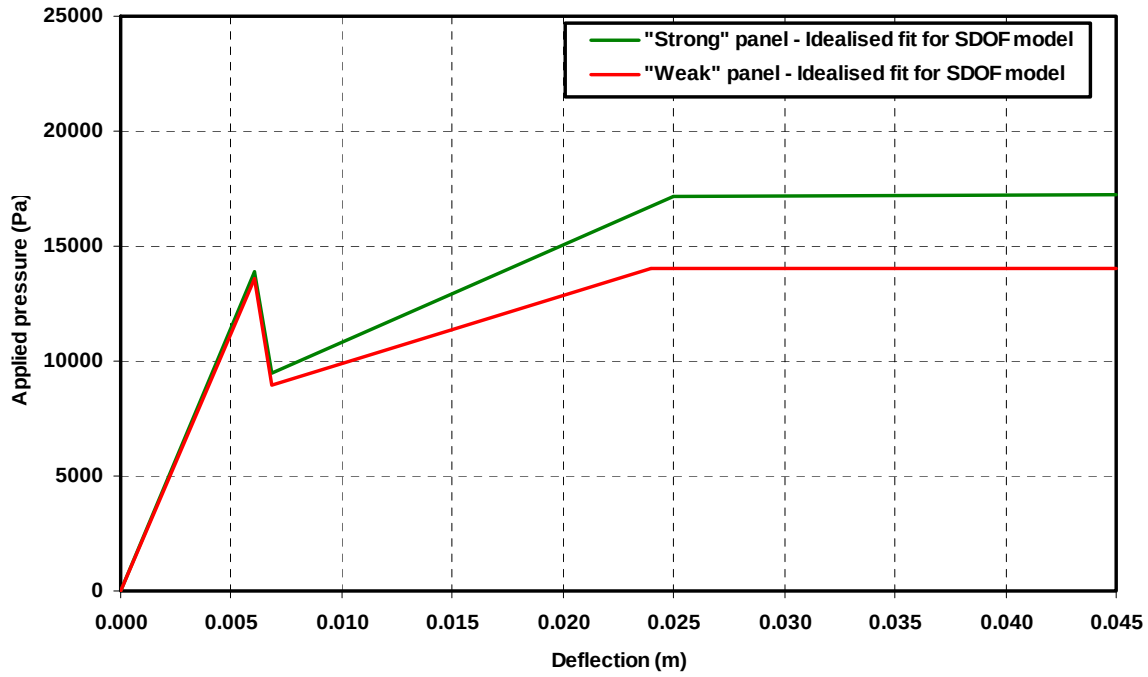

Figure 22; Pressure-deflection curves resulting from pseudo-static finite element analysis of "weak" and "strong" RC panels, idealised fitted curves for SDOF models.

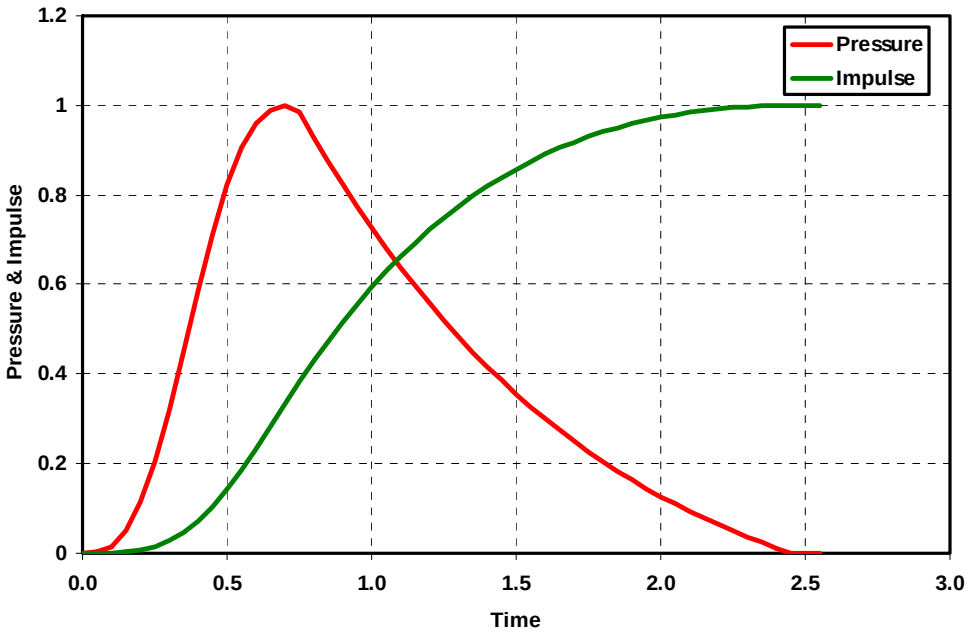

Figure 23; Unit load curve for Assumed Blast Load A.

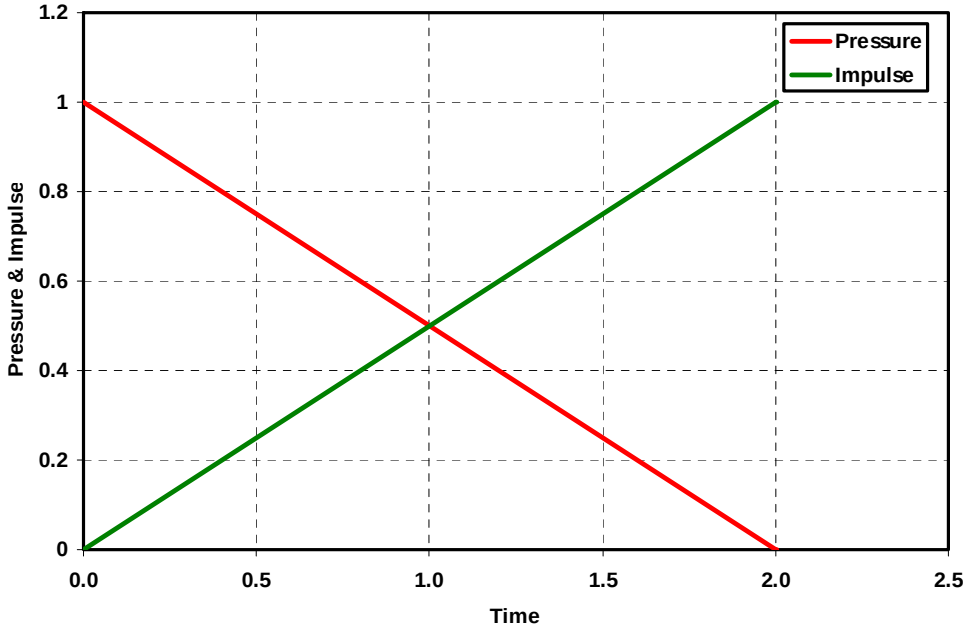

Figure 24; Unit load curve for Assumed Blast Load B.

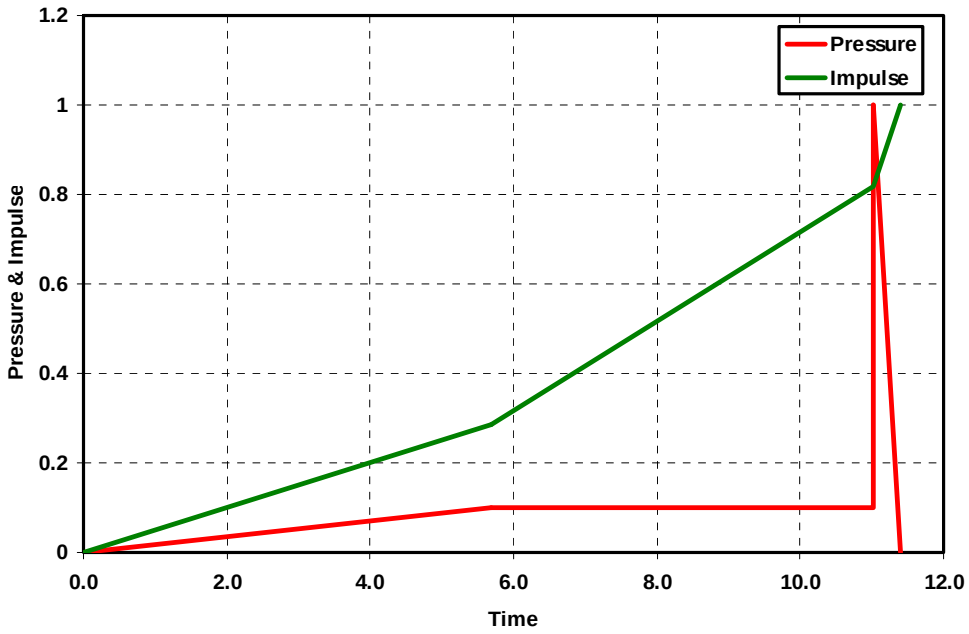

Figure 25; Unit load curve for Assumed Blast Load C.

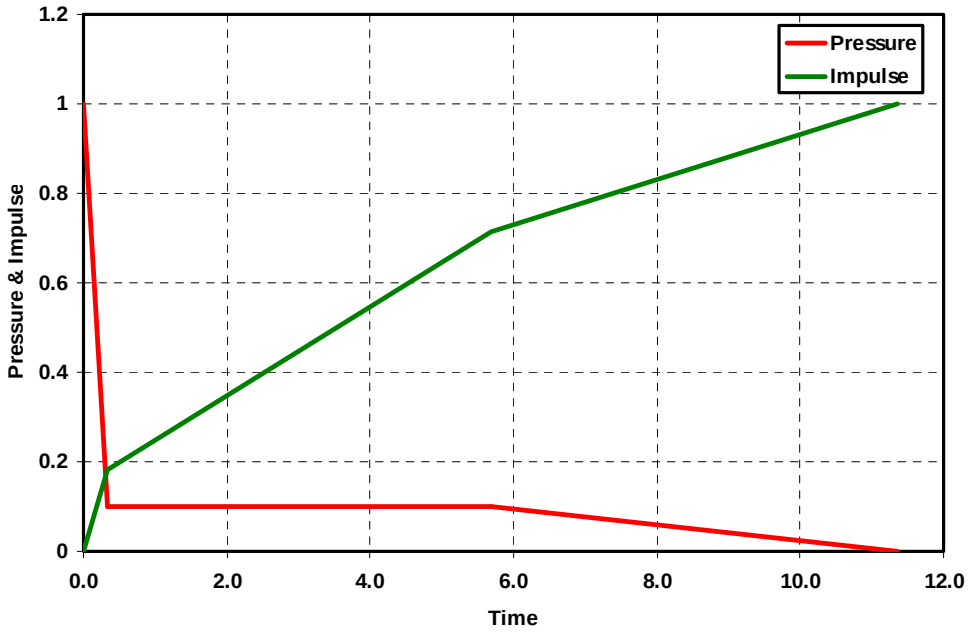

Figure 26; Unit load curve for Assumed Blast Load D.

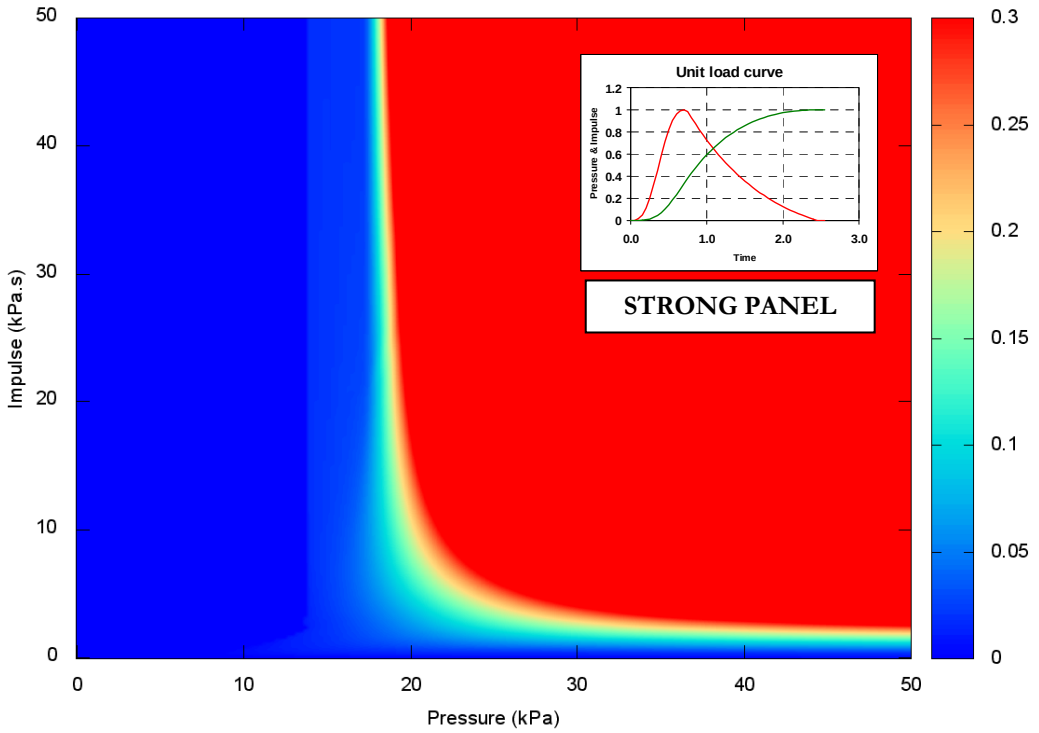

Figure 27; Permanent deflection contours predicted by SDOF model, "strong" panel, applied loading as idealised vapour/ dust explosion form (Assumed Blast Load A).

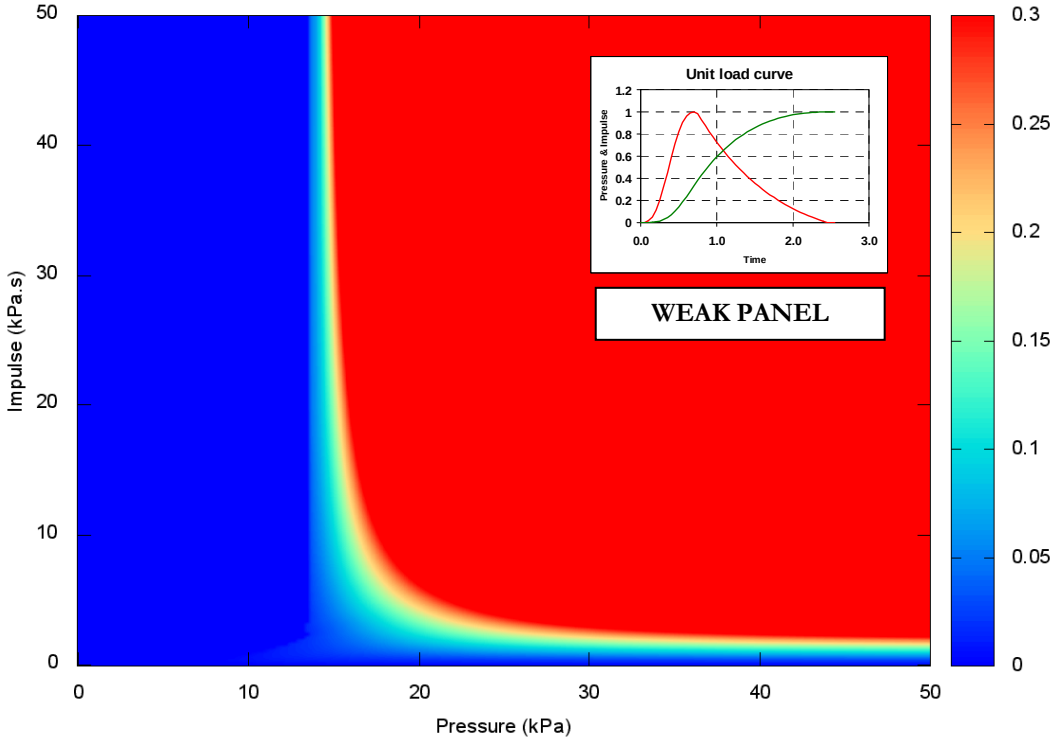

Figure 28; Permanent deflection contours predicted by SDOF model, "weak" panel, applied loading as idealised vapour/ dust explosion form (Assumed Blast Load A).

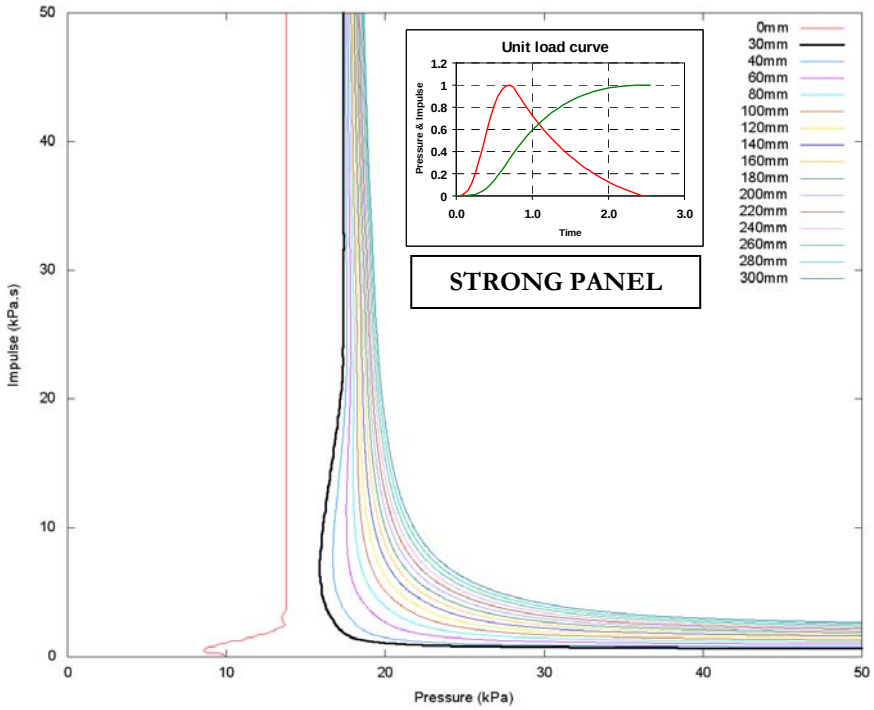

Figure 29; Iso-damage curves predicted by SDOF model, "strong" panel, applied loading as idealised vapour/dust explosion form (Assumed Blast Load A).

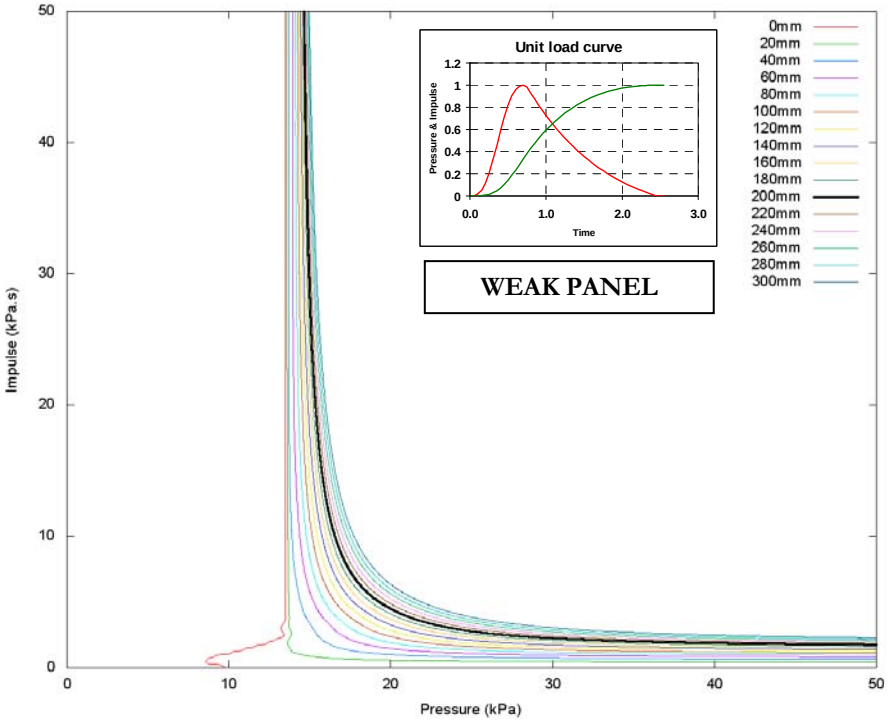

Figure 30; Iso-damage curves predicted by SDOF model, "weak" panel, applied loading as idealised vapour/dust explosion form (Assumed Blast Load A).

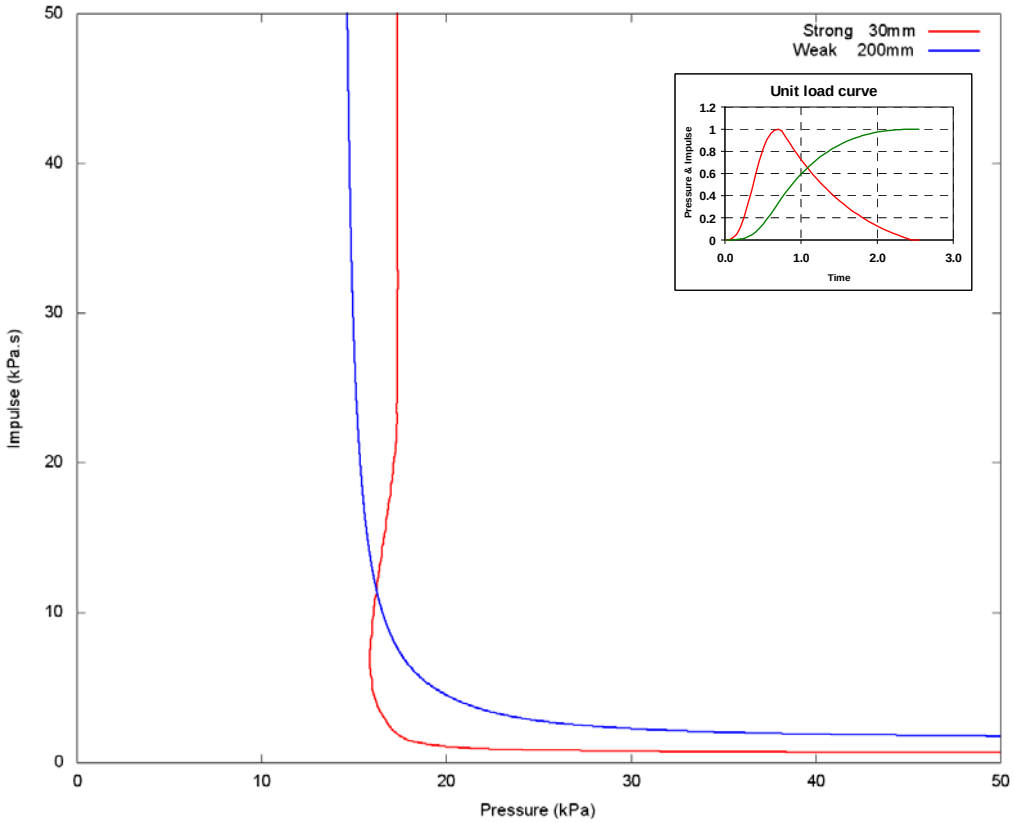

Figure 31; Iso-damage curves predicted by SDOF model, applied loading as idealised vapour/dust explosion form (Assumed Blast Load A), showing onset of failure for strong panel and 200mm permanent deflection for weak panel.

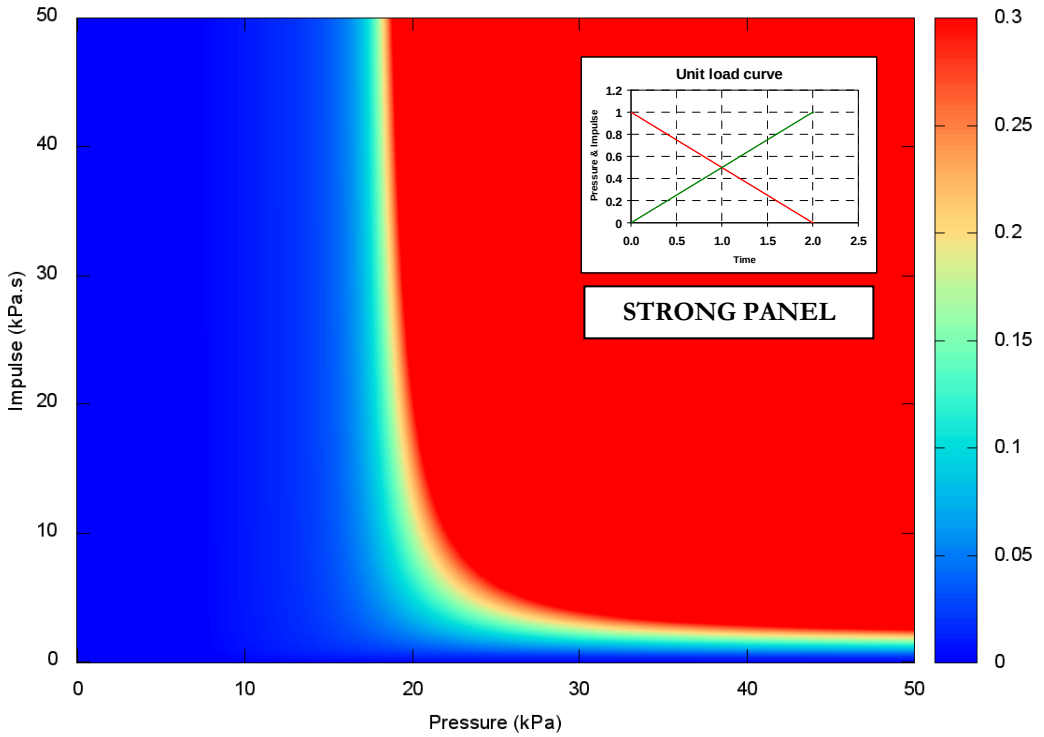

Figure 32; Permanent deflection contours predicted by SDOF model, "strong" panel, applied loading as idealised high explosive form (Assumed Blast Load B).

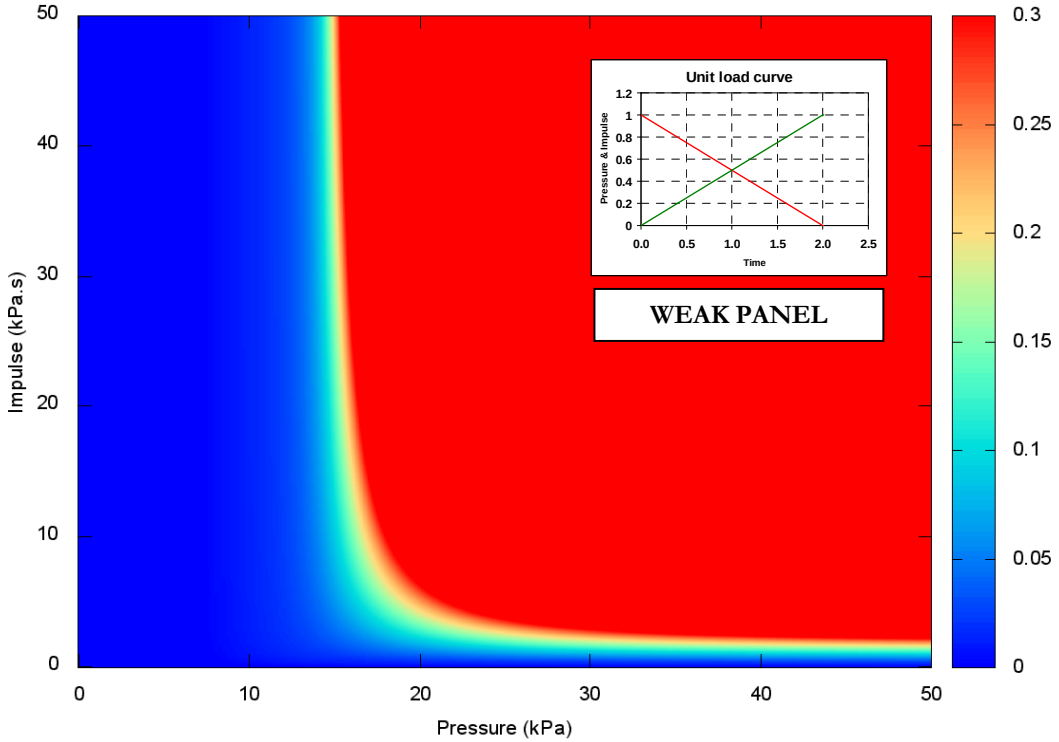

Figure 33; Permanent deflection contours predicted by SDOF model, "weak" panel, applied loading as idealised high explosive form (Assumed Blast Load B).

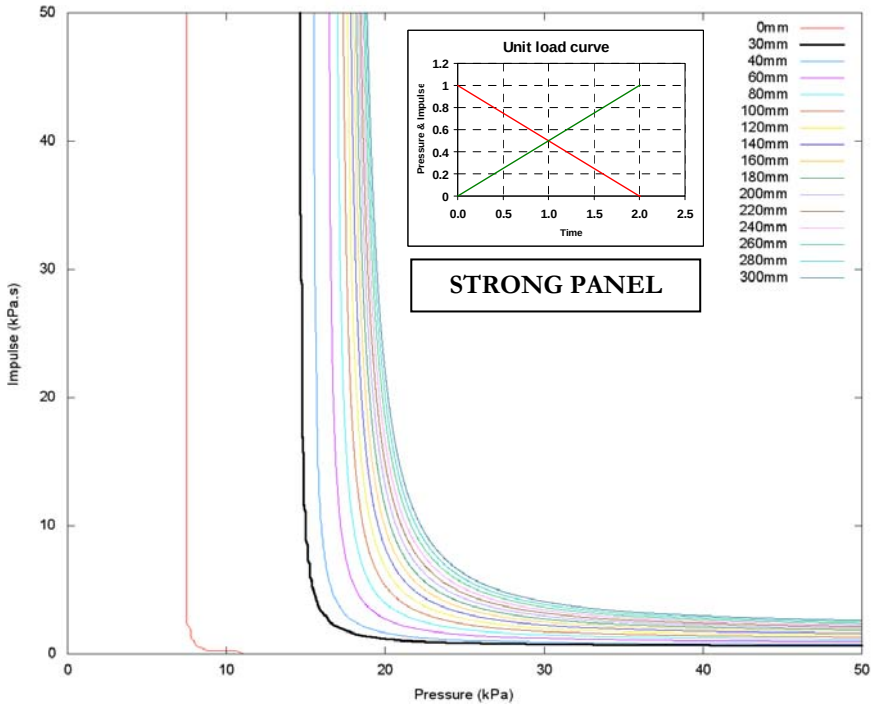

Figure 34; Iso-damage curves predicted by SDOF model, "strong" panel, applied loading as idealised high explosive form (Assumed Blast Load B).

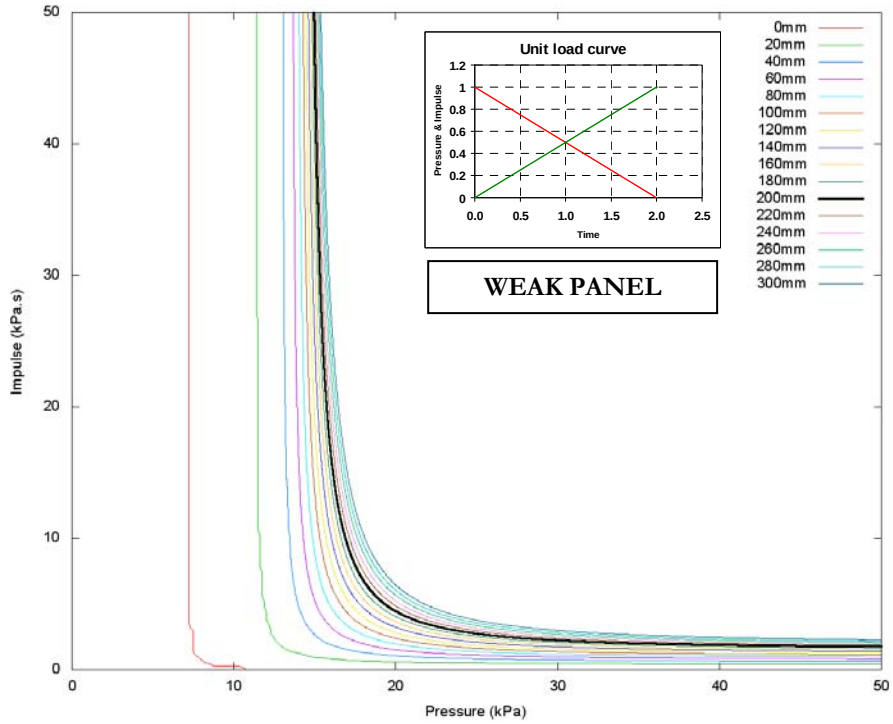

Figure 35; Iso-damage curves predicted by SDOF model, "weak" panel, applied loading as idealised high explosive form (Assumed Blast Load B).

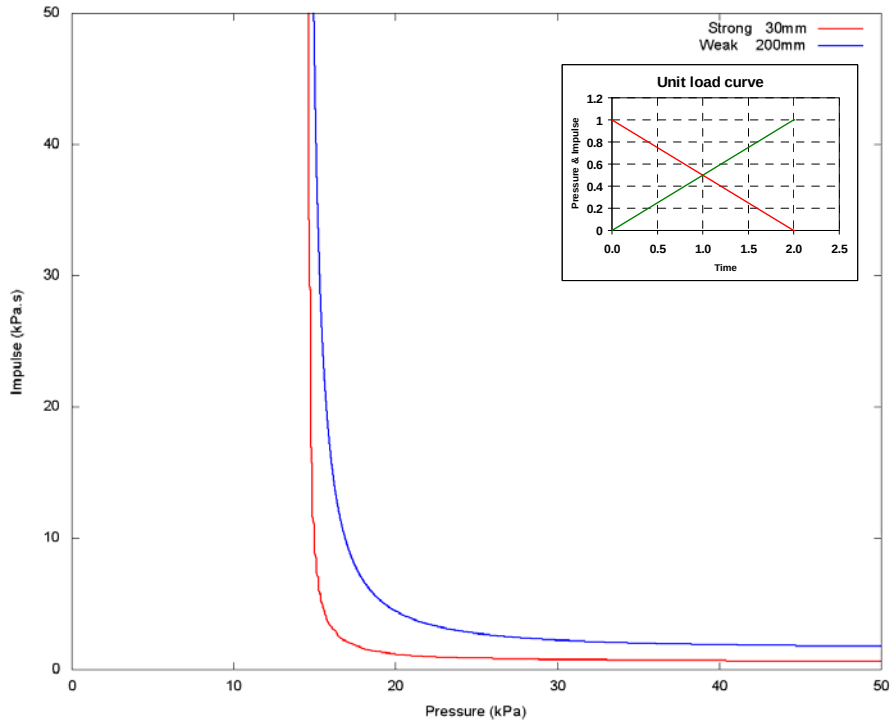

Figure 36; Iso-damage curves predicted by SDOF model, applied loading as idealised high explosive form (Assumed Blast Load B), showing onset of failure for strong panel and 200mm permanent deflection for weak panel.

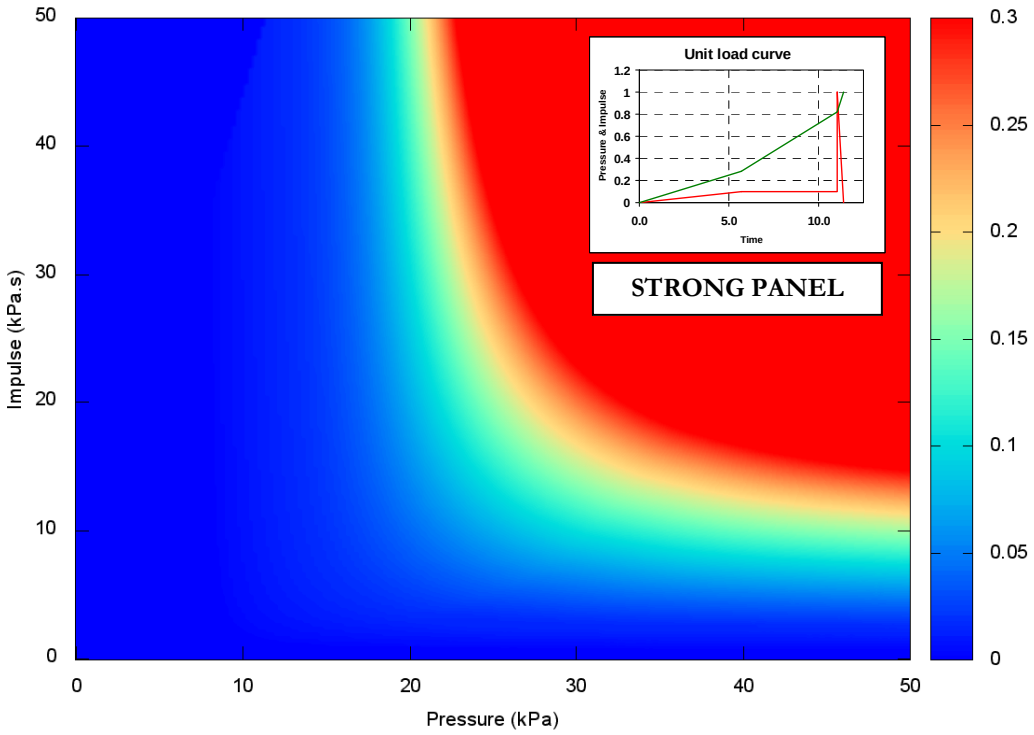

Figure 37; Permanent deflection contours predicted by SDOF model, "strong" panel, applied loading as Assumed Blast Load C.

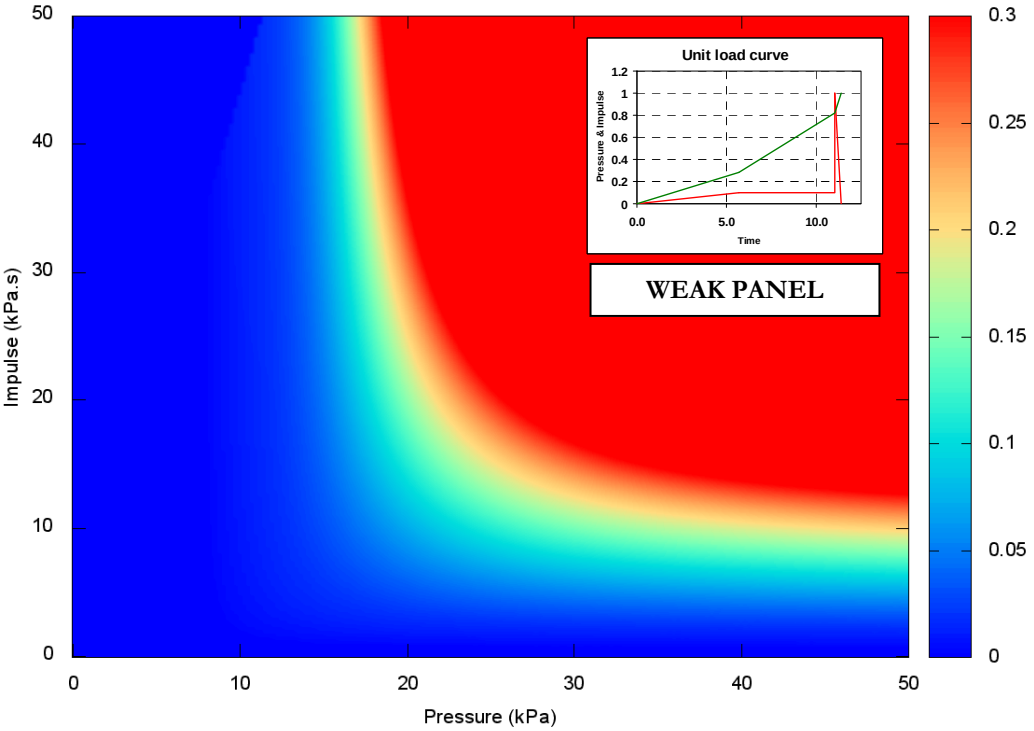

Figure 38; Permanent deflection contours predicted by SDOF model, "weak" panel, applied loading as Assumed Blast Load C.

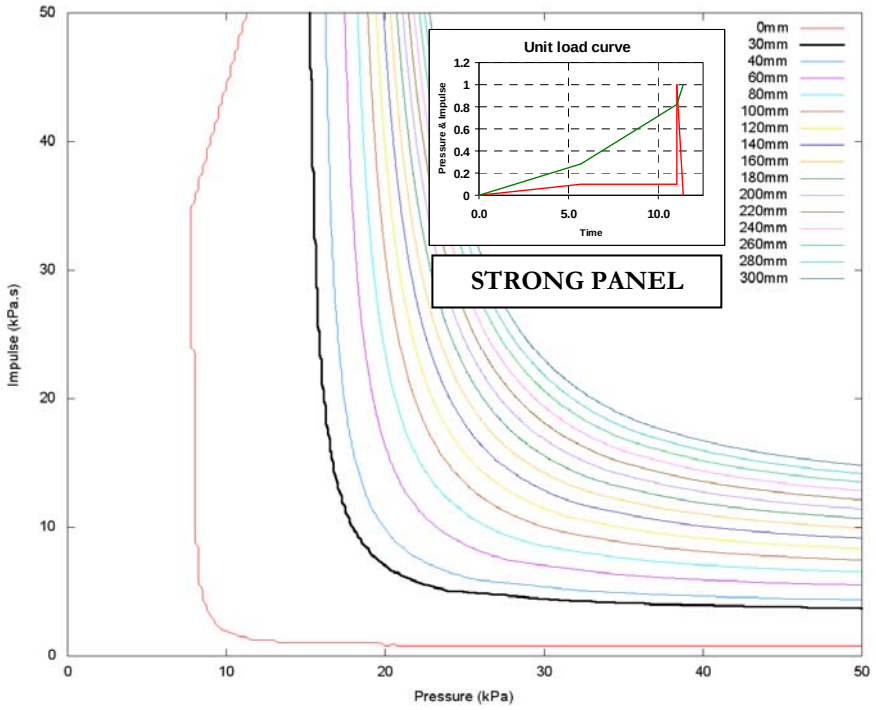

Figure 39; Iso-damage curves predicted by SDOF model, "strong" panel, applied loading as Assumed Blast Load C.

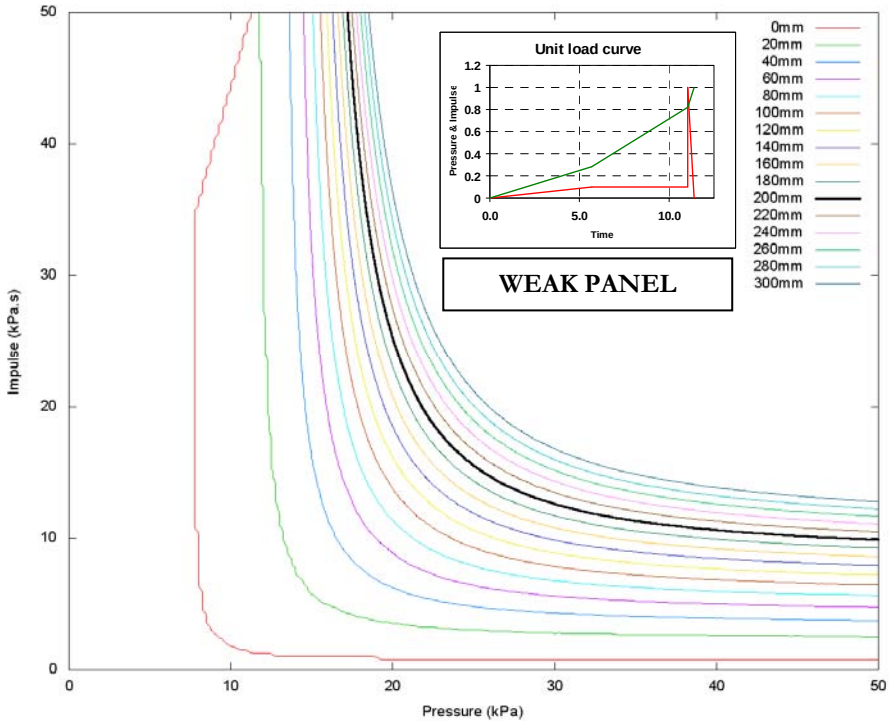

Figure 40; Iso-damage curves predicted by SDOF model, "weak" panel, applied loading as Assumed Blast Load C.

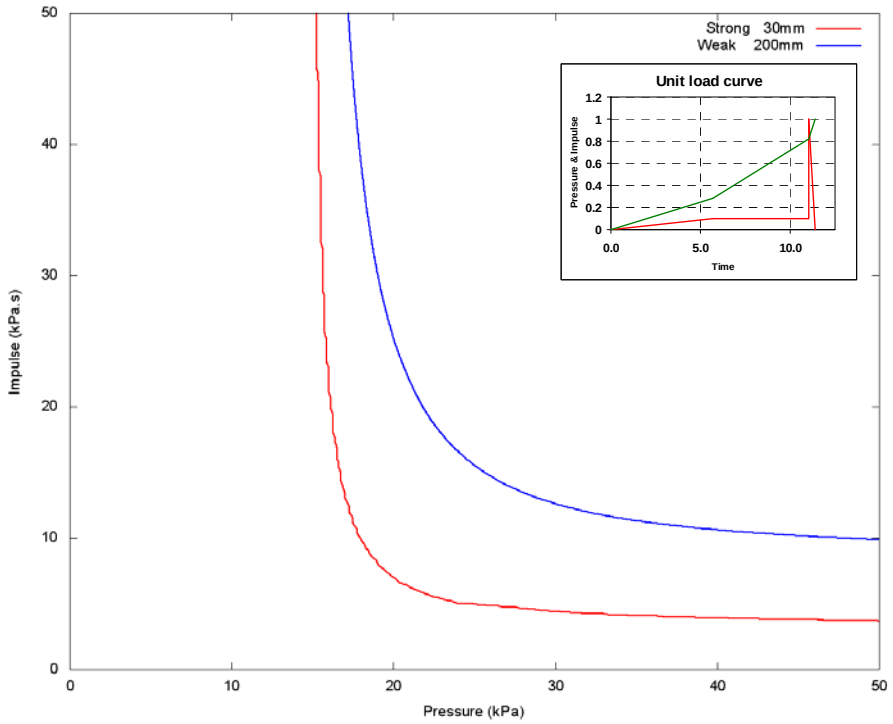

Figure 41; Iso-damage curves predicted by SDOF model, applied loading as Assumed Blast Load C, showing onset of failure for strong panel and 200mm permanent deflection for weak panel.

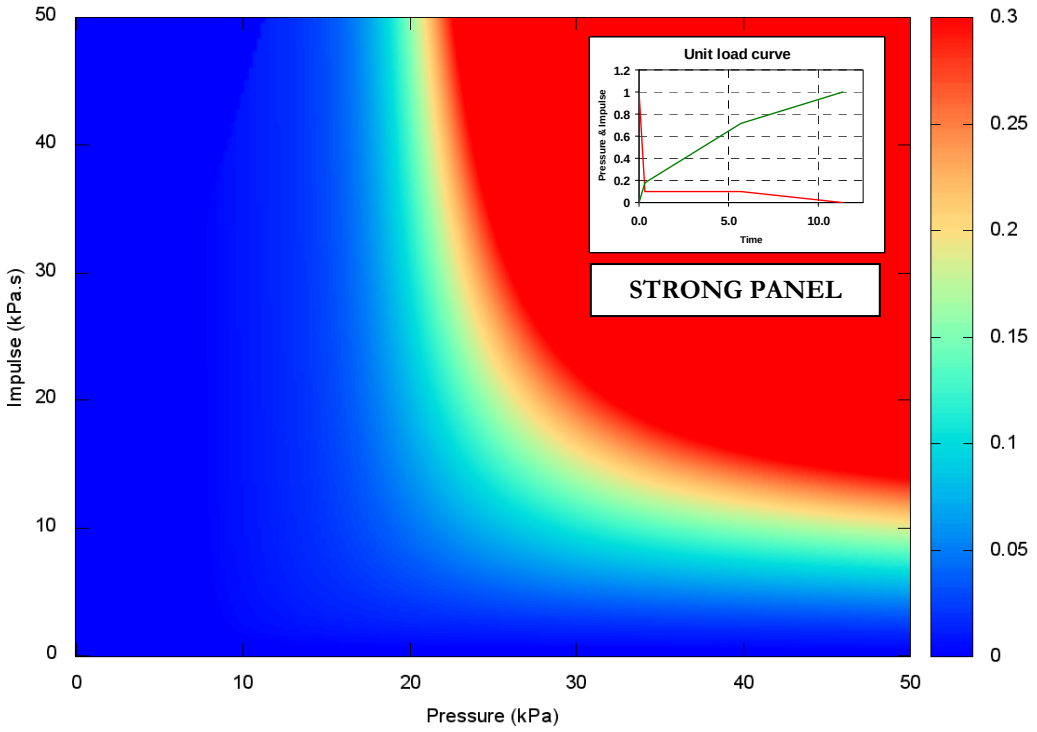

Figure 42; Permanent deflection contours predicted by SDOF model, "strong" panel, applied loading as Assumed Blast Load D

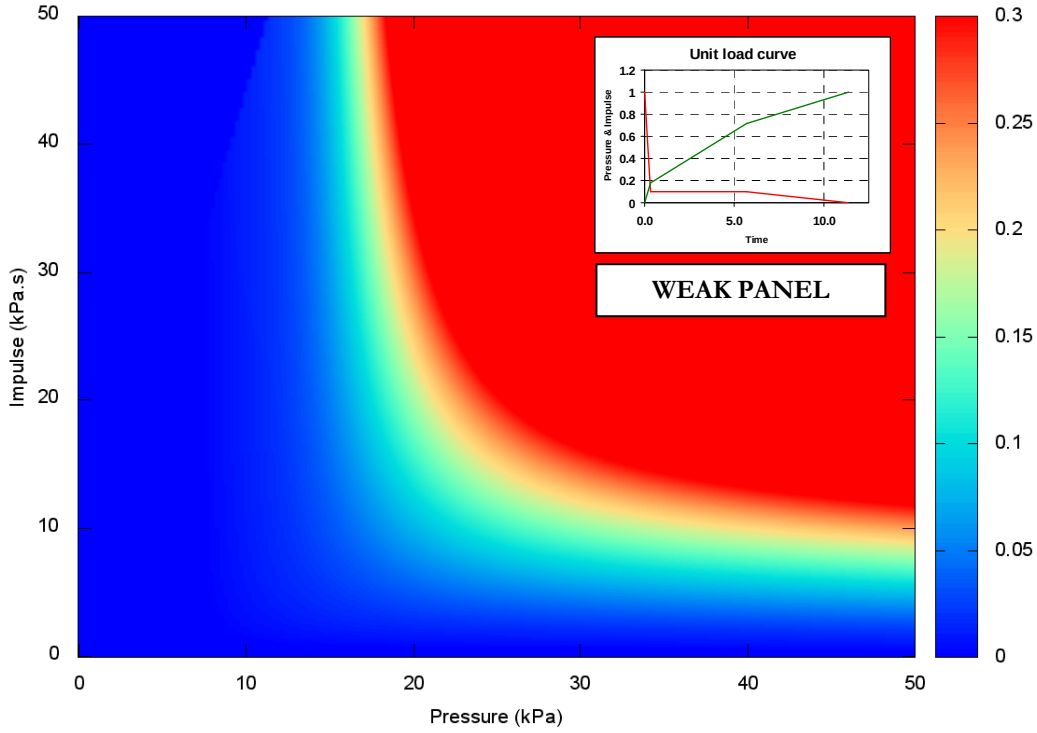

Figure 43; Permanent deflection contours predicted by SDOF model, "weak" panel, applied loading as Assumed Blast Load D.

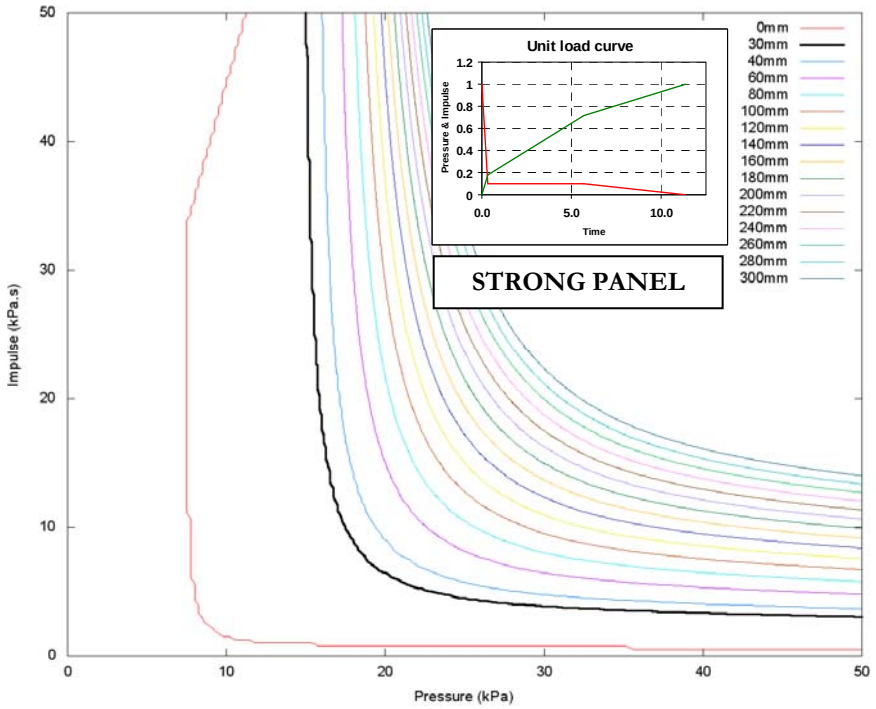

Figure 44; Iso-damage curves predicted by SDOF model, "strong" panel, applied loading as Assumed Blast Load D.

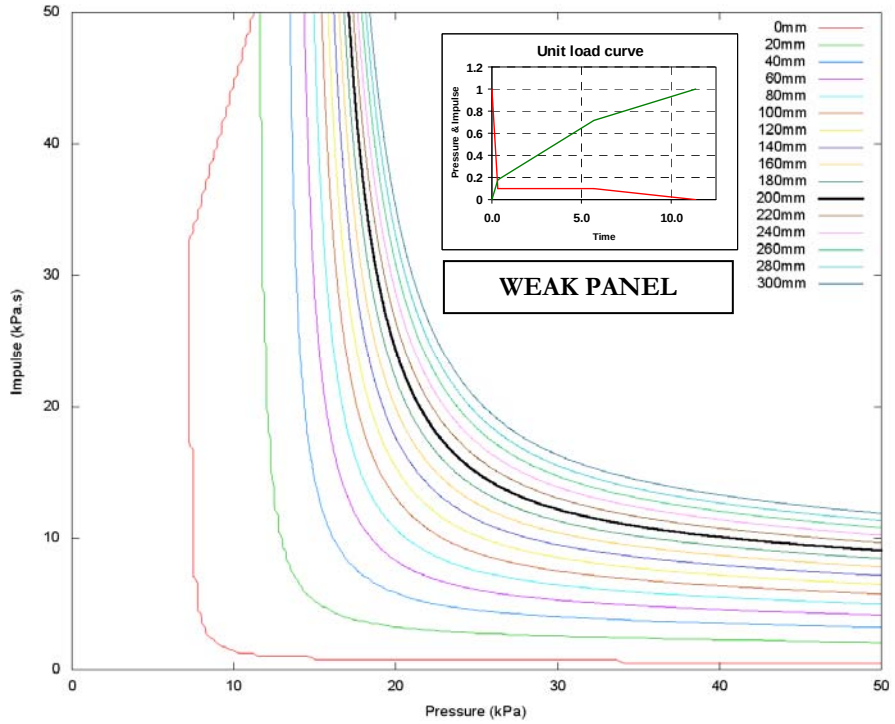

Figure 45; Iso-damage curves predicted by SDOF model, "weak" panel, applied loading as Assumed Blast Load D.

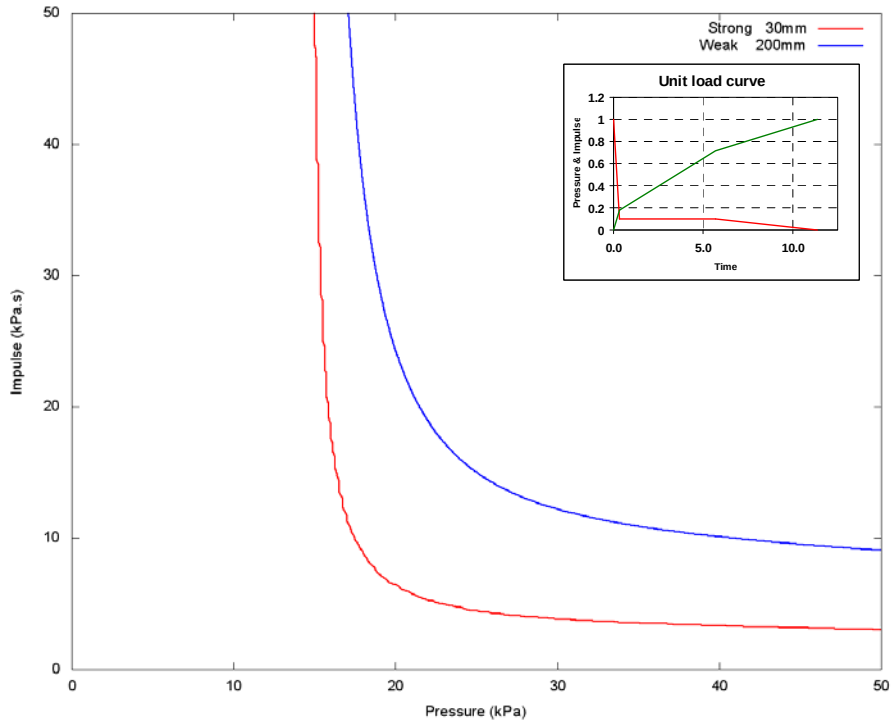

Figure 46; Iso-damage curves predicted by SDOF model, applied loading as Assumed Blast Load D, showing onset of failure for strong panel and 200mm permanent deflection for weak panel.

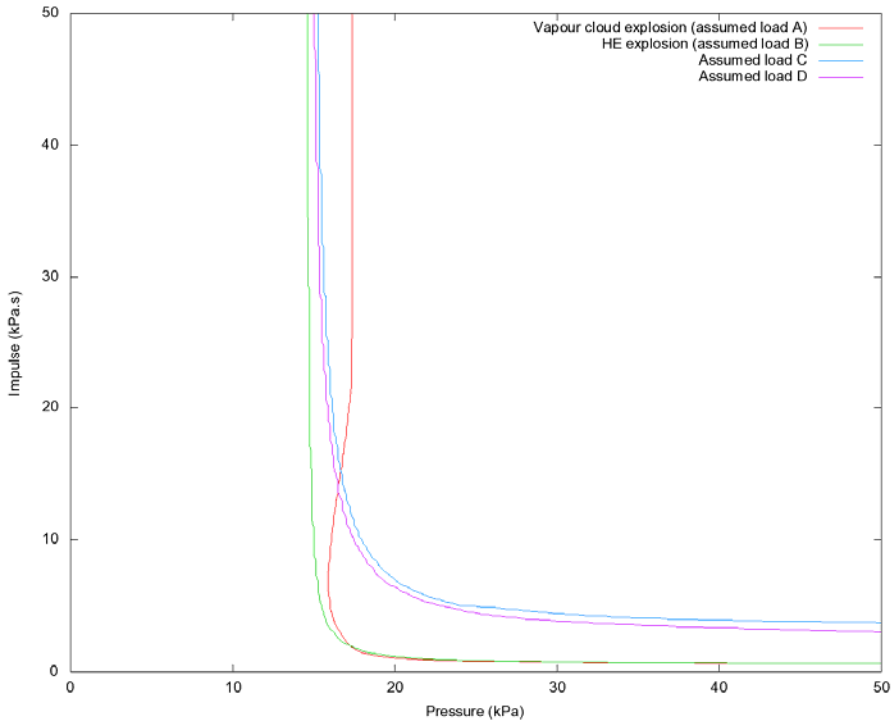

Figure 47; Iso-damage curves predicted by SDOF model, applied loading as Assumed Blast Loads A to D, showing onset of failure for strong panel.

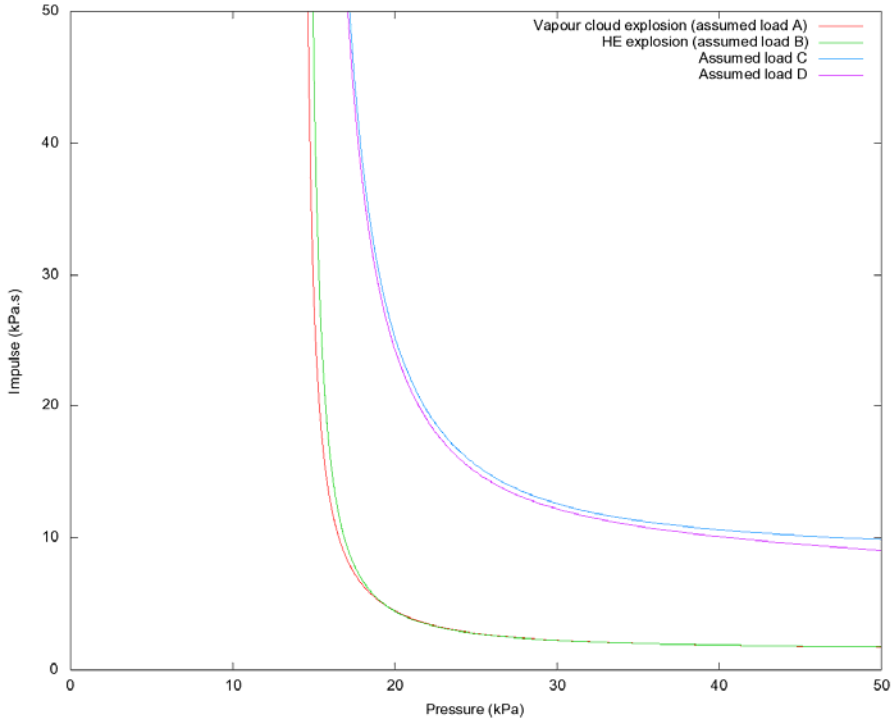

Figure 48; Iso-damage curves predicted by SDOF model, applied loading as Assumed Blast Loads A to D, showing 200mm deflection for weak panel.

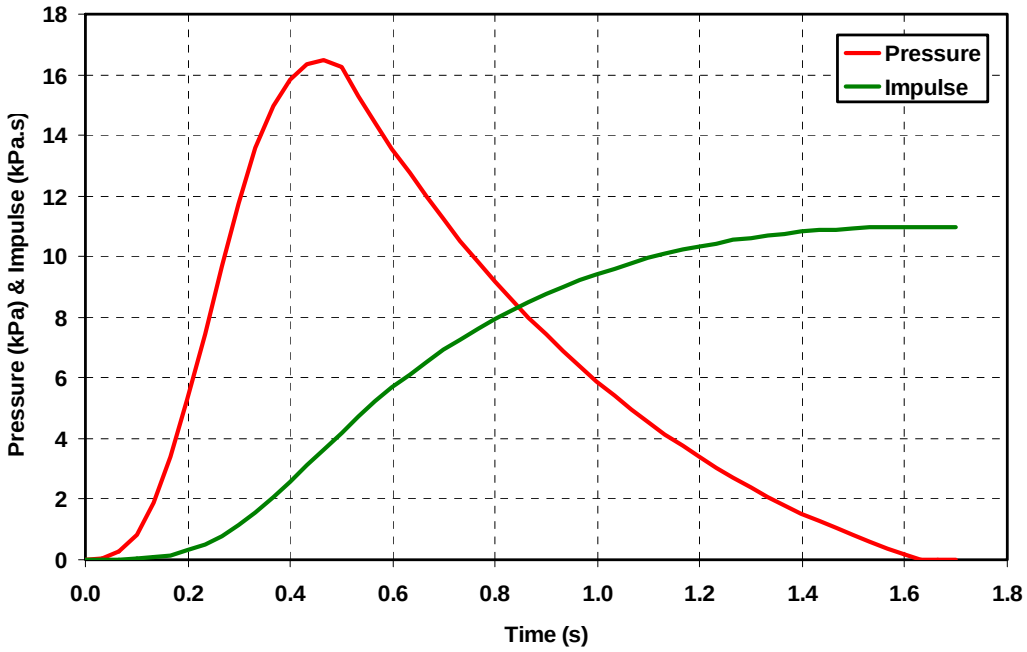

Figure 49; The only load curve which has been found to cause the observed structural response.

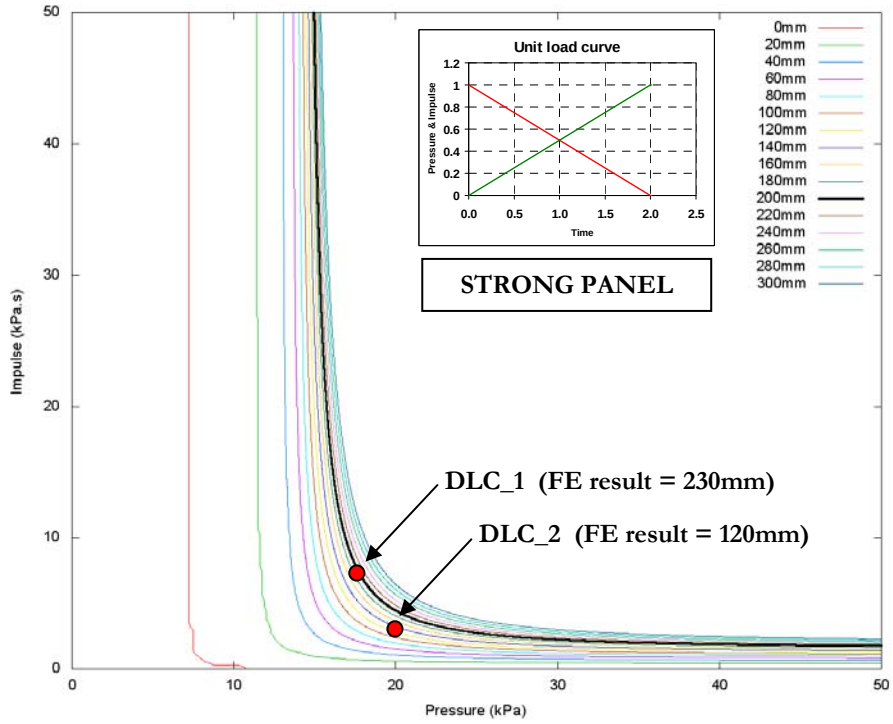

Figure 50; Iso-damage curves predicted by SDOF model, "weak" panel, applied loading as idealised high explosive form (Assumed Blast Load B), locations of DLC_1 and DLC_2 are indicated.

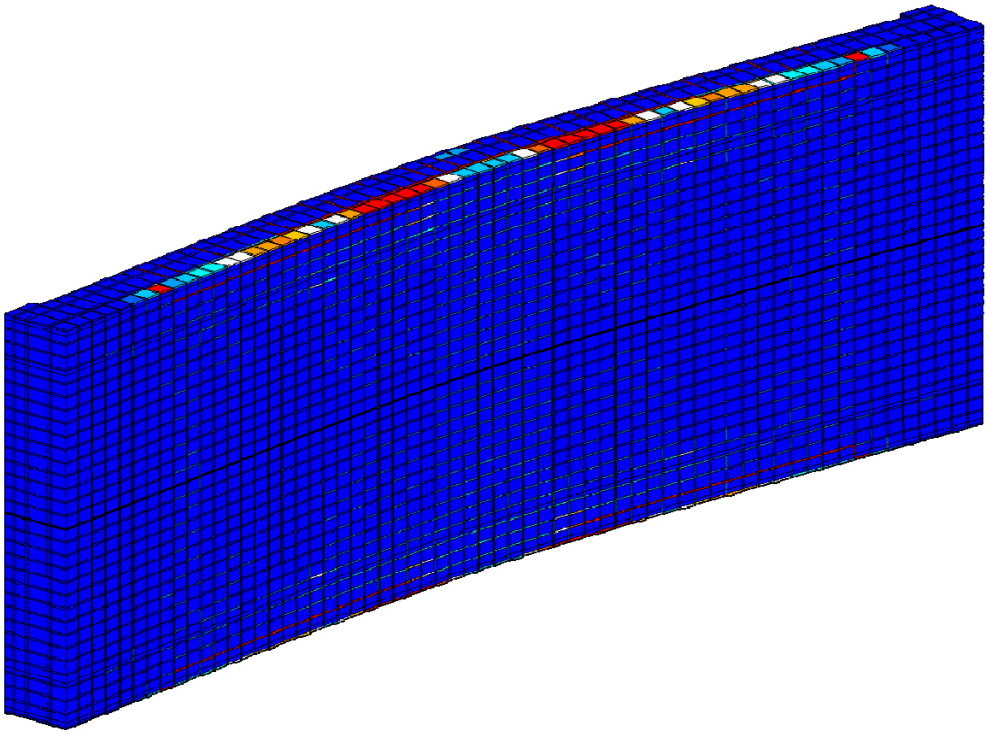

Figure 51; Finite element result, coarse model, front view, contours of damage, DLC_1.

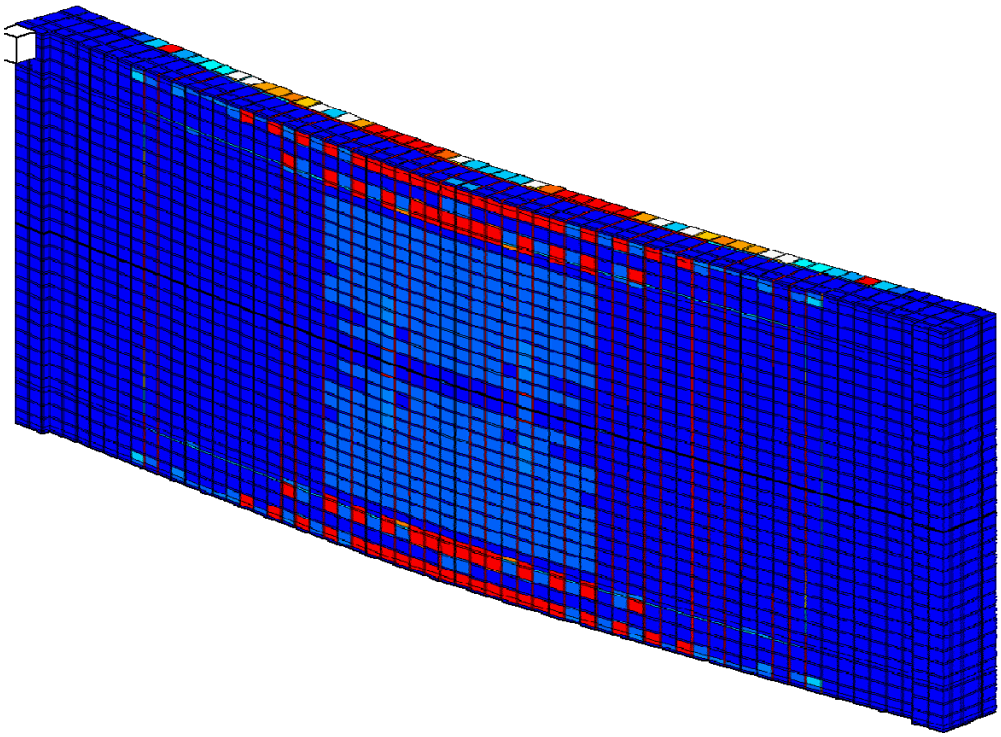

Figure 52; Finite element result, coarse model, rear view, contours of damage, DLC_1.

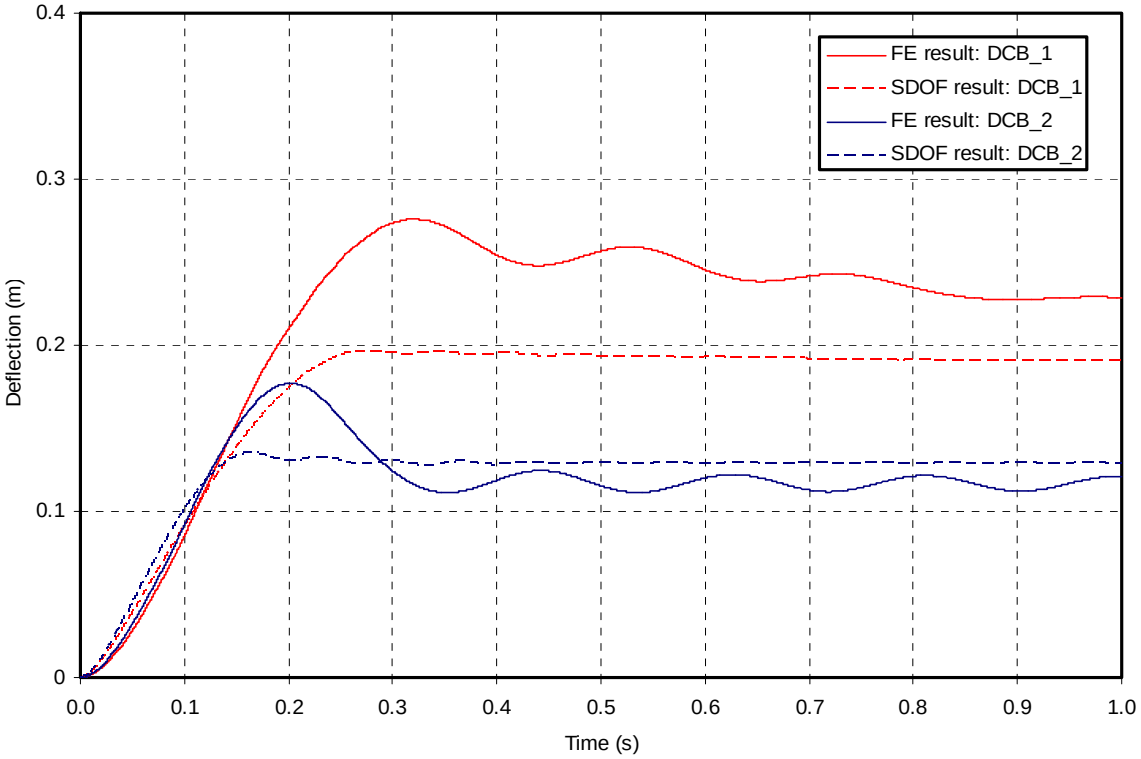

Figure 53; Displacement-vs-time results from SDOF models and FE models for DLC_1 & DLC_2.

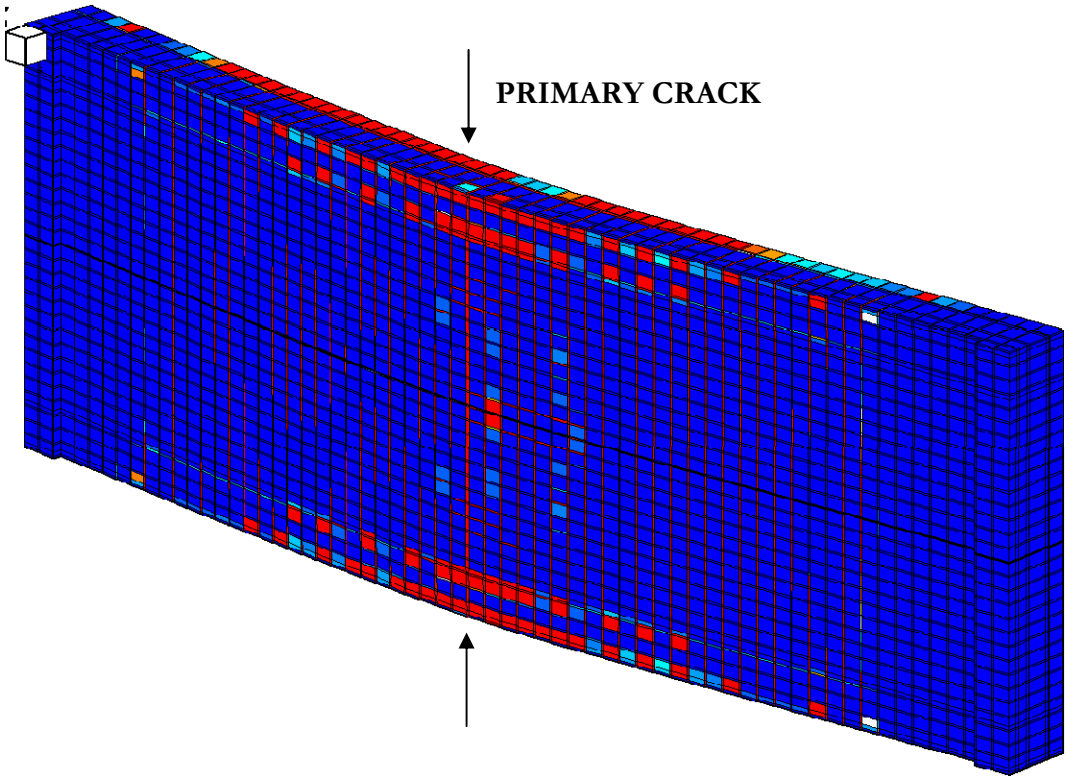

Figure 54; Finite element result, coarse model, rear view, contours of damage, DLC_3.

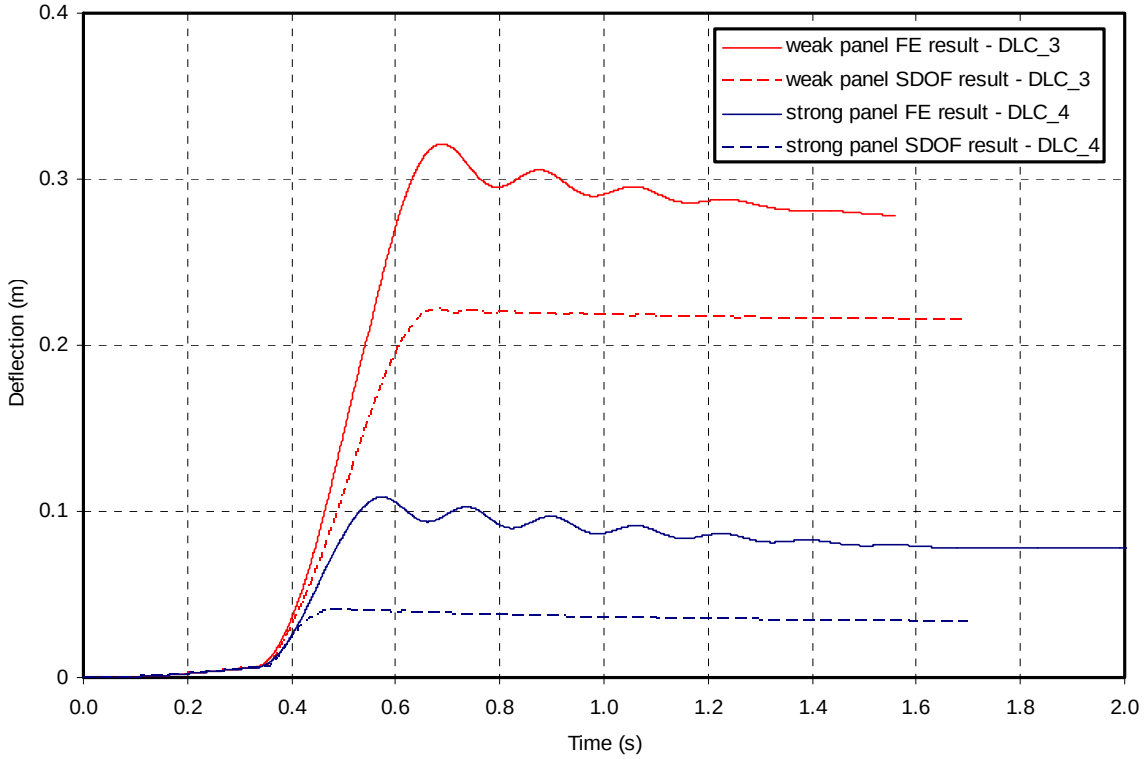

Figure 55; Displacement-vs-time results from FE models for DLC_3 & DLC_4.

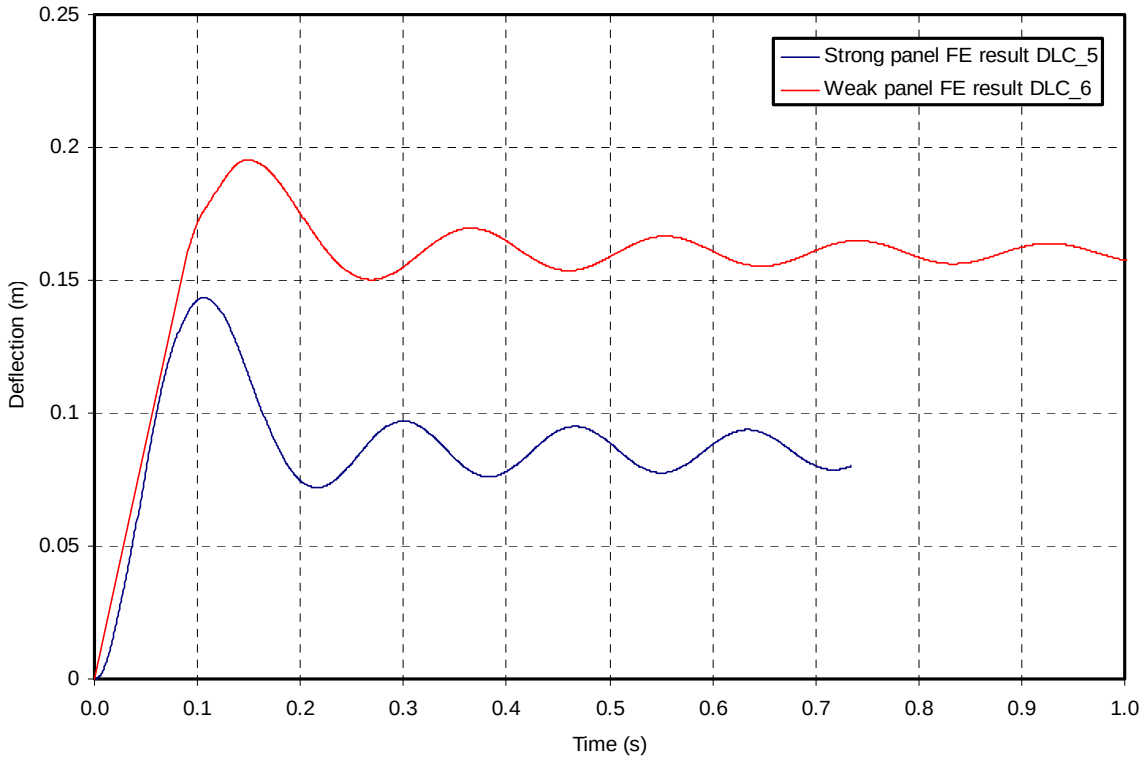

Figure 56; Displacement-vs-time results from FE models for DLC_5 & DLC_6.

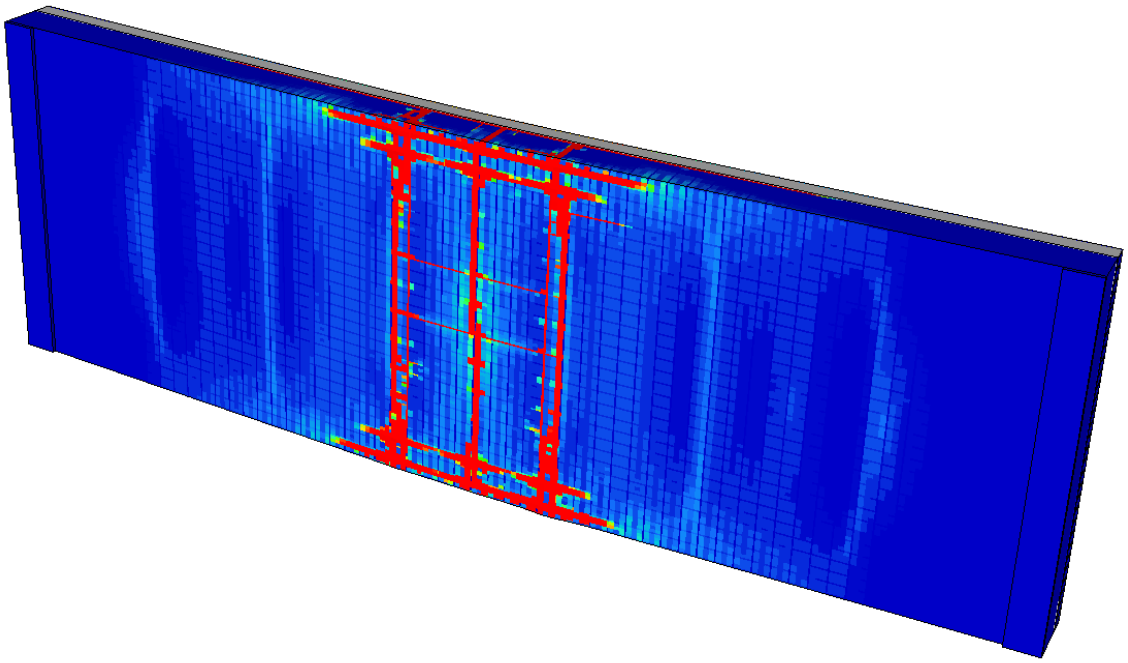

Figure 57; Finite element result, fine model, rear view, contours of damage, DLC_6.

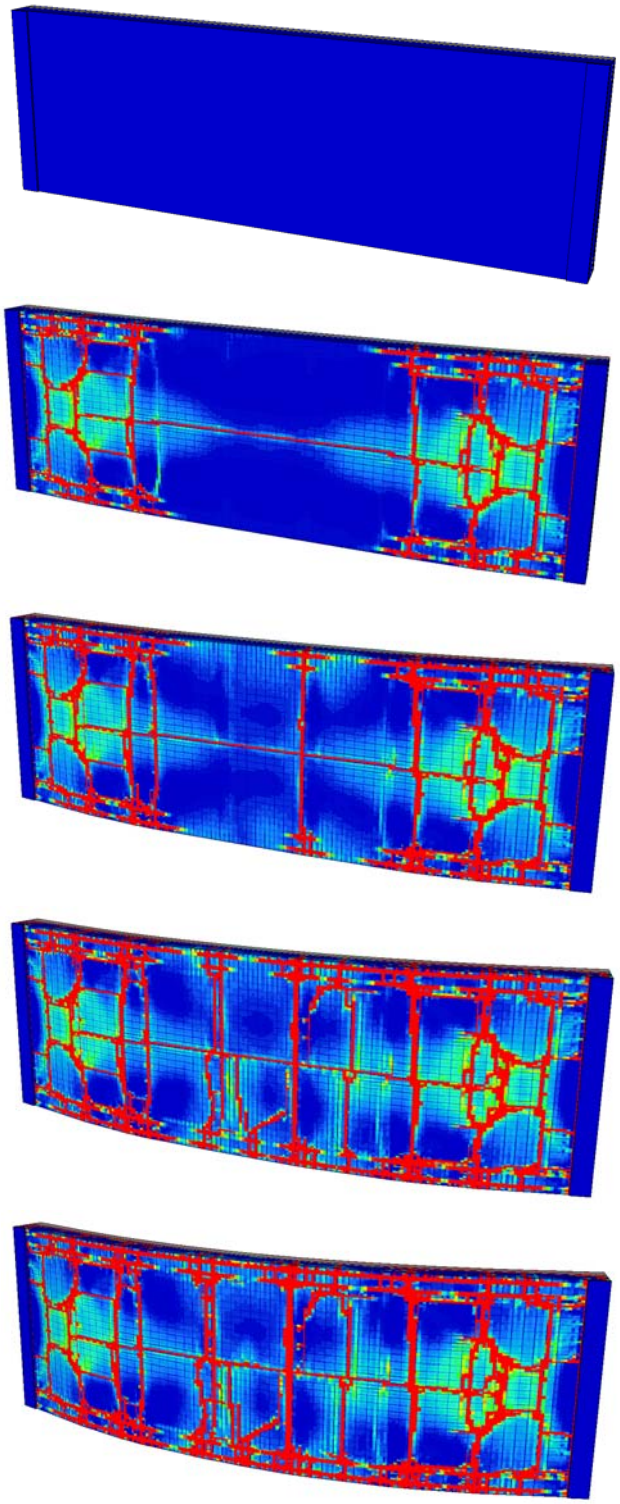

Figure 58; Finite element result, fine model, rear view, contours of damage, DLC_7, snapshots at 20msec intervals.

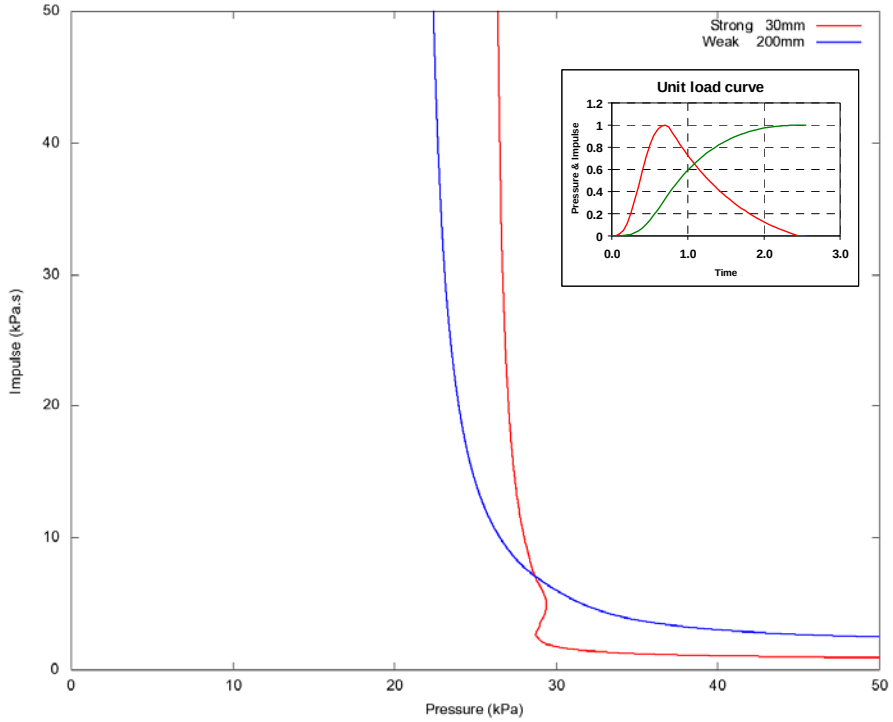

Figure 59; Iso-damage curves predicted by SDOF model, applied loading as idealised vapour/ dust explosion form (Assumed Blast Load A), showing onset of failure for strong panel and 200mm permanent deflection for weak panel, steel yield stress at 1.3xdesign values.

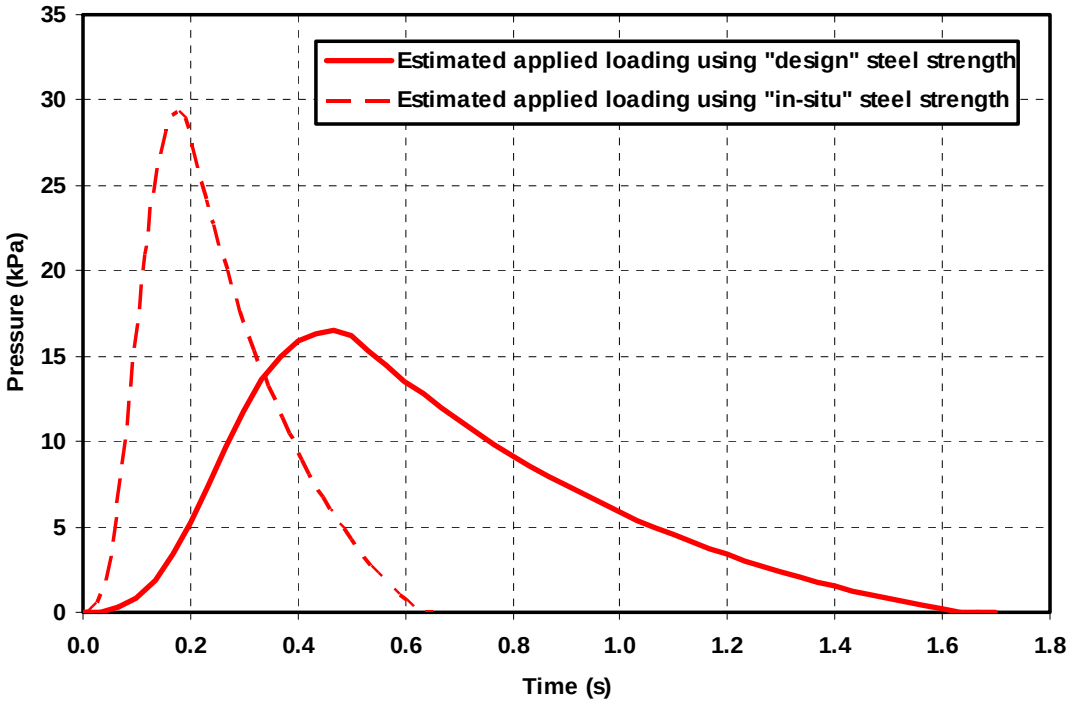

Figure 60; Load curves which have been found to cause the observed structural response using "design" and "in-situ" steel strengths.

16. ANNEX A - Hand calculations to predict the cladding panel strength

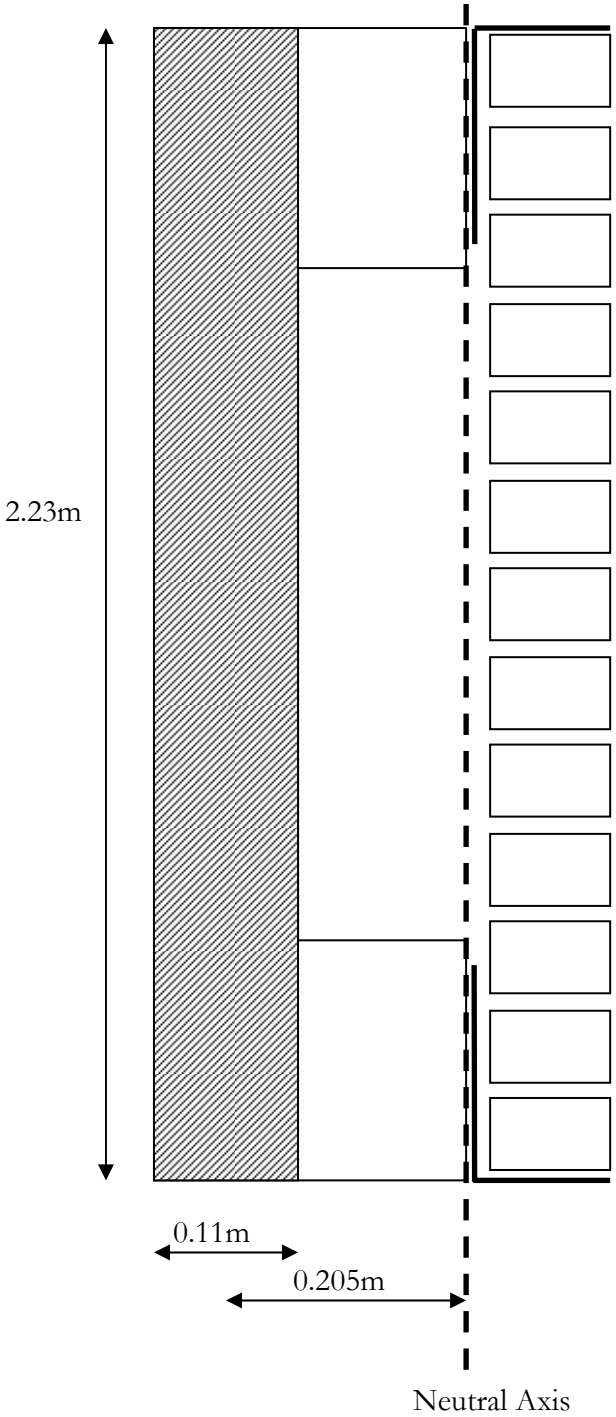

Concrete strength in tension

Assume that the panel is reinforced but not prestressed.
Assume characteristic compressive strength at time of blast is 40MPa.

Tensile strength = 2.4MPa to 4.7MPa (Use 3.5MPa)
From CEB-FIP Model Code 1990

Tensile area of concrete:
Assume slab cross section = 0.11*2.23m = 0.2453m^2

Distance from neutral axis = 0.205m
Tensile force = 3.5MPa * 0.245m^2 = 859kN

Resisting moment from concrete in tension:
= 859*0.205
= 176 kN.m

For a 7m span and a UDL this gives applied pressure to fracture concrete:
= 8M/2.23L^2
= (8*176)/(2.23*7^2)
= 12.9kPa

So the back of the panel will fracture when the applied pressure reaches approximately 13kPa.

Once the concrete fractures all tension is carried by rebar.

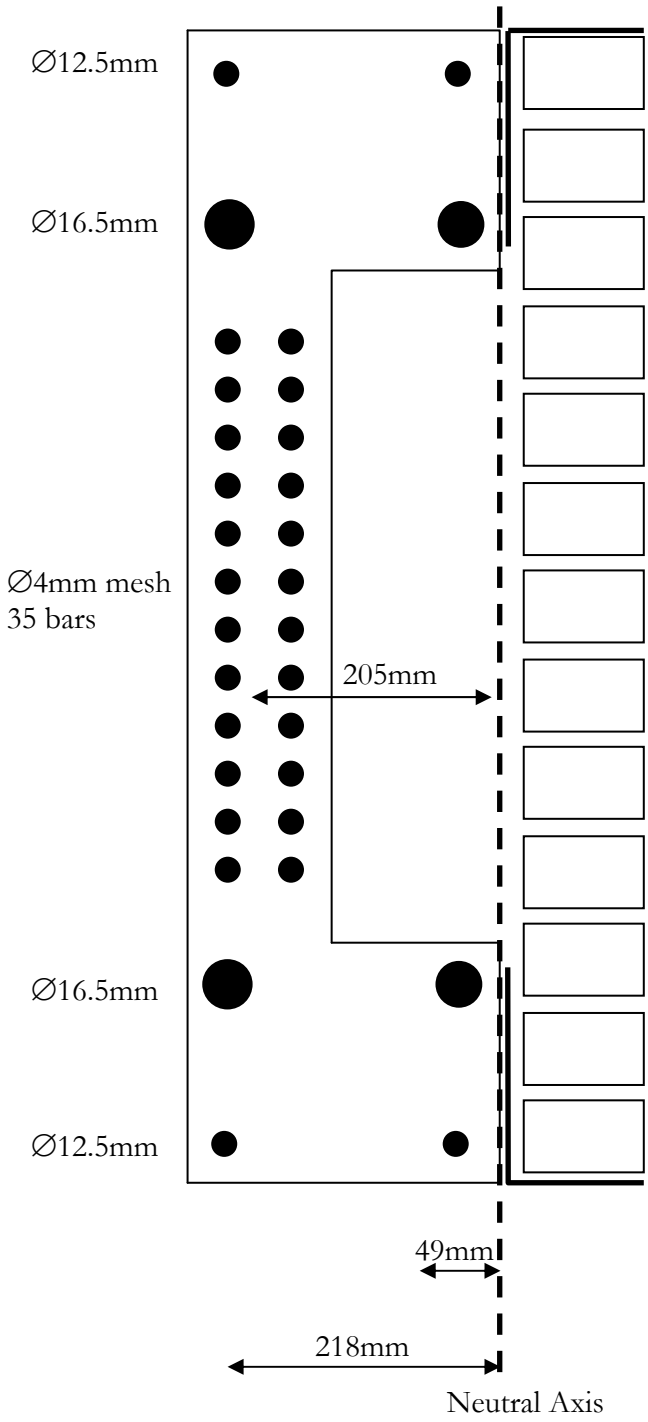

Steel strength in tension (weak slab)

Assume that the neutral axis as at the interface between the steel angle section and the concrete.

Assuming a yield stress of 250MPa:

Resisting moment =
$2*(0.25*PI*(0.0125^2+0.0165^2)*250e6)*(0.049+0.218)+$
$PI*0.25*0.004^2*35*0.205*250e6$
= 44929+22541
= 67.5kN.m

For a 7m span and a UDL this gives applied pressure to yield the steel:
$= 8M/2.23L^2$
$= (8*67.5)/(2.23*7^2)$
= 4.95kPa

Assuming a yield stress of 460MPa:
Applied pressure to yield the steel:
= 4.95*(460/250)
= 9.01kPa

Best estimate of rebar yield is about 9kPa for the weak panel.

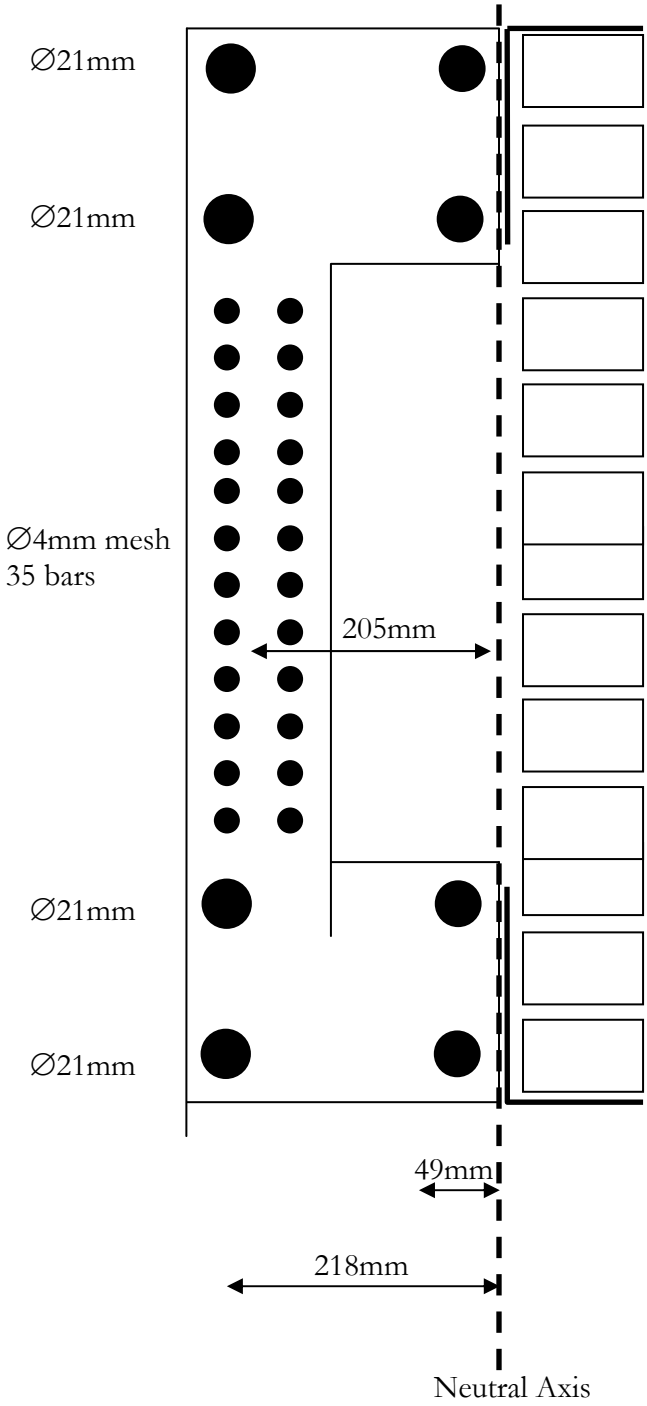

Steel strength in tension (strong slab)

Assume that the neutral axis as at the interface between the steel angle section and the concrete.

Assuming a yield stress of 250MPa:

Resisting moment =
$2*(0.25*PI*(0.021^2+0.021^2)*250e6)*(0.049+0.218)+$
$PI*0.25*0.004^2*35*0.205*250e6$
= 92478+22541
= 115.0kN.m

For a 7m span and a UDL this gives applied pressure to yield the steel:
$= 8M/2.23L^2$
$= (8*115)/(2.23*7^2)$
= 8.42kPa

Assuming a yield stress of 460MPa:
Applied pressure to yield the steel:
= 8.42*(460/250)
= 15.49kPa

Best estimate of rebar yield is about 15.5kPa for the strong panel.